Acoustic source levels associated with the nonlinear interactions of ocean waves

A. C. Kibblewhite and C. Y. Wu
Department of Physics, University of Auckland, Auckland, New Zealand

(Received 22 May 1992; revised 11 August 1993; accepted 11 August 1993)

Spectra of wave-induced microseismic noise are calculated as a function of the distance from the center of an active wave region of finite size, to examine the influence of the inhomogeneous component of the pressure field arising from nonlinear wave interactions in a shallow water environment. The contribution of this component is shown to be very dependent on the properties of the bottom structure, especially the rigidity of the top sedimentary layer and the shear-wave velocities of the sublayers. Calculations for a typical six-layered bottom with an overlying unconsolidated sediment in a shallow water environment (100-m water layer) confirms that the inclusion of the inhomogeneous component of the pressure field can raise the total seismic spectral level up to 30–40 dB, as indicated recently by Schmidt and Kuperman [J. Acoust. Soc. Am. **84**, 2153–2162 (1988)] in an analysis of "bottom magnification." When the bottom is composed of a solid half-space, however, this contribution is found to drop to only a few dB. It is also demonstrated that for the multilayered model being discussed the contribution from the inhomogeneous component drops quickly and by as much as 30 dB, when the observation point is moved outside the active region. These results confirm the interpretation of the ULF noise-source levels, reported earlier by Kibblewhite and Ewans [J. Acoust. Soc. Am. **78**, 981–994 (1985)] on the basis of onshore microseismic spectra, and show why they are reasonably representative of the wind-dependent ULF noise spectra observed in deep water.

PACS numbers: 43.30.Nb, 43.30.Ma

INTRODUCTION

It is now well established that at ultra low frequencies (ULF) the ocean surface wave field, the underwater noise field, and the seismic activity at the sea floor are all closely related to each other. The central part of this interrelationship is the nonlinear interaction between components of the surface wave field. These interactions generate an acoustic pressure field which in turn produces the seismic response in the sedimentary structure of the seabed.[1,2]

The literature of the 1960s is rich with accounts of associated contributions—see Ref. 3 for a review of these—but a renewed interest in ULF seismoacoustics in the 80s has resulted in a series of more recent publications based on vastly improved technology.[3–12] Among these was our contribution, Ref. 3, reported in 1985. In this experiment the seismic response was recorded, not at the seabed, but at an onshore site close to the region of wave activity. In this respect the experiment suffers in comparison with the excellent deep-water measurements, reports of which began to appear at about the same time, but the long-term nature of the recordings and the quality of the supporting environmental data give the New Zealand experiment a particular significance. Among the results reported were a set of wind-dependent ULF pressure spectra derived from the seismic spectra recorded on shore. The spectral levels reported were consistent with other measurements reported at that time. Further the spectra, and their behavior with wind speed, appeared to conform very closely to the predictions of wave-interaction theory.

While satisfying, the significance of this agreement with theory was uncertain for various reasons. For instance because the observation point in the New Zealand experiment was, in terms of the dominant acoustic wavelength, close to the active wave region, it had been assumed that the wave-induced seismic activity as measured on shore would not differ significantly from that within the active region itself, and that the inversion of the seismic spectra recorded onshore would give a reasonable representation of the off-shore acoustic pressure field. Further the geoacoustic environment was approximated by a simple two-layered fluid model so that the most elementary transfer function was used in the inversion. These assumptions required justification before the true significance of the New Zealand spectra could be properly assessed.

A first step in providing the clarification needed began with a re-examination of the assumptions made in the earlier analysis.[8,9] In these studies we employed a two-layered viscoelastic model and established a revised transfer function for the case when the seismic response on shore was made up of both a diffracted field and a contribution from an interface wave. Transfer functions were calculated for two versions of the two-layered model—one involving an unconsolidated and the other a solid half-space. While the pressure spectra derived from the seismic spectra using these revised transfer functions still showed close agreement with the predictions of wave-interaction theory, it was clear that uncertainty would persist until the effects of near-field propagation and a multi-layered bottom structure were incorporated in the transfer function. Other issues also required attention. For instance most recent analyses[5,6,7,10,12] have involved deep-water situations in which the inhomogeneous component of the wave-induced pressure field can usually be ignored. However, restricting consideration to the homogeneous component alone needs proper justification through a more complete analysis of the wave-interaction mechanism.

The importance of such studies has been highlighted recently by Schmidt and Kuperman.[10] In an analysis of surface-generated ambient noise in a horizontally stratified environment, they virtually demonstrated the marked influence, not previously well recognized, which the inhomogeneous component can have on noise levels at low frequencies. They argue that a significant part of the spectral variation of seismoacoustic noise in shallow water can be the result of such propagation effects and the excitation of interface waves. They correctly emphasise that the influence of such environmental effects should be removed in any inter-comparison of ULF noise spectra recorded at different sites. In relation to the New Zealand spectra[3,4] in particular, they suggest that, as the observed levels may be enhanced by as much as 40 dB due to seabed "magnification" alone, the observed peak in the noise spectrum at low frequencies may be as much due to propagation effects as ocean-wave processes.

This conclusion, if correct, has obvious implications regarding the role of wave–wave interactions as the source of the main peak in the ULF seismoacoustic spectrum. The New Zealand spectral levels are consistent with ULF noise data measured at deepwater sites and show a wind dependence in line with wave-interaction theory. If the source levels interpreted on the basis of the New Zealand experiment are some 40 dB too high, as Schmidt and Kuperman's analysis suggests, much of the evidence for the acoustic role of the wave–wave interaction process is placed in question. The overall evidence available does not support such a conclusion.

We believe that the resolution of the question raised by Schmidt and Kuperman lies in a better understanding of the source, the bottom-response function and of the dependence of the seismic field on the position of the observation point relative to the active wave region. Theoretical studies to establish the pressure and seismic field arising from wave–wave interactions have usually considered the seismoacoustic response either inside the active region or so far from it that only a few interface wave modes are involved in the propagation of energy. In the first of these scenarios the active region is considered infinite in size and elegant expressions for the spectra of the pressure/seismic fields are established in terms of plane-wave solutions. In the second the observation point is considered to be at a very large distance compared with the dimensions of an active region of finite size, and the formal solution is obtained by application of the theorem of residuals. The intermediate range situations which are of practical importance, particularly in respect of wave activities on the continental shelf, have not been examined. To address these cases two specific extensions to existing theory are still required. The first involves a full discussion of the inhomogeneous component of the wave-induced pressure field and the second a study which examines the behavior of the seismic response of a multi-layered seabed when a seismic sensor is moved beyond the boundaries of an active region through the near field to the far field outside it. Further evidence of this need comes from the recent work of Hedlin and Orcutt.[11] Reporting on long term averages of microseismic spectra recorded at island sites, they show that the observed spectral levels of the double-frequency seismic noise are usually lower on shore than those observed nearby in the ocean, the difference appearing to vary from site to site.

This paper, with its companion,[12] attempts to provide this analysis. In Ref. 12 we extended the theory governing wave–wave interactions to include, inter alia, an examination of the properties of the inhomogeneous component of the wave-induced pressure field under various conditions. In the present paper we use these developments to examine the seismo-acoustic response of a multi-layered environment to the wave-interaction process, both inside and outside the active region. The theoretical analysis developed in Ref. 12 is used in Sec. I as the basis of an analysis to establish an expression for the seismic spectrum inside an active region of finite size. In Sec. II we show that this expression devolves to the classical formula when the size of the active region becomes infinite and the horizontal wave number is restricted to ω/α_1. In Sec. III we discuss the numerical calculation of the spectral transfer function and examine its characteristics in a multi-layered environment when the active wave region is infinite in size. In Sec. IV the Green's function is used to establish expressions for the three components of the microseismic field as a function of distance from the center of an active region of finite size, for liquid, solid and multi-layered representations of the New Zealand environment. We have used this structure (and versions of it) to allow straightforward comparison with the analysis in Ref. 10. In a paper in preparation, in which we introduce the general ocean-wave dispersion relation into wave-interaction theory, we present wind-dependent spectra for deep and shallow-water environments using more traditionally accepted models of the geostructure. Section V presents the results of numerical calculations of the vertical component of the seismic response for the various models, the results for the two horizontal components and a discussion of their application in bottom property investigations being left to the later paper. Section VI interprets the original New Zealand spectra in the light of the results for the vertical component and examines the question raised in Ref. 10 regarding the source levels for the wave–wave interaction process. Confining discussion to the vertical component is appropriate given the purposes of the present paper. A short summary is given in Sec. VII. The errors introduced to make the computer-intensive numerical calculations tractable are discussed in Appendix A.

I. A GENERAL EXPRESSION FOR THE MICROSEISM SPECTRUM

We now consider a modification of the classical expression for the wave-induced microseism spectrum to include the influence of both the inhomogeneous component of the pressure field and an active region of variable size. In this context, we consider the idealized situation in which the active region is taken to be an area on which a uniform ocean-wave field is acting, outside of which the sea surface is assumed to be calm.

By introducing the Green's functions, $G_v(\mathbf{r},\mathbf{r}_0)$, $G_h(\mathbf{r},\mathbf{r}_0)$, linking the vertical and horizontal displacements of an element of the sea floor at a point $\mathbf{r}$ to a point source at $\mathbf{r}_0$, the total vertical/ horizontal displacement at $\mathbf{r}$ can be expressed as:

$$u_{v,h}(\omega,\mathbf{r})=\int_S p(\mathbf{r}_0,\omega)G_{v,h}(\mathbf{r},\mathbf{r}_0)\,d\mathbf{r}_0\,,$$

where $\mathbf{r}_0 \in S$. It can be shown that the Green's function takes the form

$$G_{v,h}(\mathbf{r},\mathbf{r}_0)=\int_0^\infty f_{v,h}(u)J_0(u\xi)u\,du, \tag{1}$$

where u ($\equiv k\alpha_1/\omega$) is the relative (horizontal) wave number, $\xi=|\mathbf{r}-\mathbf{r}_0|\,\omega/\alpha_1$ is the relative distance,

$$f_v(u)=\frac{i\omega}{2\pi\rho_1\alpha_1^3}\frac{1-R_b}{1+R_b}\sqrt{1-u^2}, \tag{2}$$

and

$$f_h(u)=f_v(u)R_{hv}(u), \tag{3}$$

where $R_b=R_b(u,\omega)$ is the bottom reflection coefficient, and $R_{hv}(u)$ is the ratio of the horizontal and vertical displacements.

Since the horizontal component of the particle displacement at the water/seabed interface does not satisfy the continuity condition, the function $f_h(u)$ must be derived from the seismic field in the bottom (a fact critical to the derivation of the corresponding Green's functions). The ratio $R_{hv}(u)$ can be established as

$$R_{hv}(u)=\frac{-iu}{n_b}\left[\frac{n_b^2-2u^2}{n_b\sqrt{n_a^2-u^2}}\frac{(+)_p}{(-)_p}-2\frac{\sqrt{n_b^2-u^2}}{n_b}\frac{(-)_s}{(+)_s}\right], \tag{4}$$

where

$$n_b=\alpha_1/\beta_2,\quad n_a=\alpha_1/\alpha_2\,, \tag{5}$$

$$(\pm)_p=\exp\left(-\frac{\omega h_2}{\alpha_1}\sqrt{n_a^2-u^2}\right)\pm\varepsilon_p\exp\left(\frac{\omega h_2}{\alpha_1}\sqrt{n_a^2-u^2}\right), \tag{6}$$

$$(\pm)_s=\exp\left(-\frac{\omega h_2}{\alpha_1}\sqrt{n_b^2-u^2}\right)\pm\varepsilon_s\exp\left(\frac{\omega h_2}{\alpha_1}\sqrt{n_b^2-u^2}\right). \tag{7}$$

Here, α_2, β_2, and h_2 are respectively the compressional and shear-wave speed in the sedimentary layer and its thickness, ε_p is the ratio of the upward to the downward components of the compressional wave, and ε_s is that for the shear-wave components in the top sedimentary layer of the seabed. When the seabed can be regarded as an homogeneous half-space, $\varepsilon_p=\varepsilon_s=0$.

As was mentioned above, we restrict the discussion below to the spectra of the vertical displacement. First we note that in the case of an elastic half-space, the vertical response $f_v(u)$ becomes[13]

$$f_v(u)=\frac{i\omega}{2\pi\rho_1\alpha_1^3}\frac{B(u)}{A(u)}\sqrt{1-u^2}, \tag{8}$$

where

$$A(u)=\frac{\rho_2}{\rho_1}\sqrt{1-u^2}\{4u^2\sqrt{(n_a^2-u^2)\,(n_b^2-u^2)}+(n_b^2-2u^2)^2\}$$

and

$$B(u)=n_b^4\sqrt{n_a^2-u^2}.$$

In the case of a liquid bottom, $f_v(u)$ simplifies to

$$f_v(u)=\frac{i\omega}{2\pi\rho_2\alpha_1^3}\sqrt{n_a^2-u^2}. \tag{9}$$

Here and later we denote ρ_n, α_n, β_n, Q_{an}, Q_{bn} as the density, compressional, and shear-wave speeds, and the Q values of the nth layer, noting that the actual attenuation values prevailing in sediments at ultra-low frequencies are still the subject of investigation.[14]

Assuming some energy-dispersion mechanism, we can regard the movement of the sea floor under a wave-induced pressure field as a stationary stochastic process, characterized by a variance density spectrum,[15]

$$\begin{aligned}F_{mv}^{(2)}(\omega,\mathbf{r})&=\frac{\langle|du_v(\omega,\mathbf{r})|^2\rangle}{d\omega}\\&=\frac{1}{d\omega}\left\langle\left|\int d\mathbf{k}\int_s dp(\mathbf{k},\omega)E_p(k,\omega,-h_1)\right.\right.\\&\qquad\left.\left.\times e^{i\mathbf{k}\mathbf{r}_0}G_v(\mathbf{r},\mathbf{r}_0)d\,\mathbf{r}_0\right|^2\right\rangle,\end{aligned}$$

where

$$\begin{aligned}E_p(k,\omega,-h_1)&=E_p(k,\omega,z)\,|_{z=-h_1}\\&=\frac{1+R_be^{i2k_1'(z+h_1)}}{1+R_be^{i2k_1'h_1}}e^{-ik_1'z}=\frac{1+R_b}{1+R_be^{i2k_1'h_1}}e^{ik_1'h_1}\end{aligned}$$

and

$$k_1'=\sqrt{\frac{\omega^2}{\alpha_1^2}-k^2}=\frac{\omega}{\alpha_1}\sqrt{1-u^2}.$$

The subscript (2), here and later, indicates the second-order wave–wave interaction. By introducing the spectral representation of the source pressure field generated by wave–wave interactions,[8,12]

$$f_{p0}^{(2)}(\mathbf{k},\omega)=\frac{\langle|dp(\mathbf{k},\omega)|^2\rangle}{d\mathbf{k}d\omega}$$

$$=\frac{1}{2}\,\omega\rho_1^2g^2F_a^2\left(\frac{\omega}{2}\right)I^{(2)}(u,\theta_k,\omega), \qquad (10)$$

where $F_a^2(\omega/2)$ is the wave-spectrum level at half the seismic frequency, and $I^{(2)}(u,\theta_k,\omega)$ takes the form shown in Appendix B, the above seismic spectrum can be expressed more explicitly as

$$F_{mv}^{(2)}(\omega,\mathbf{r})=\frac{\omega^5g^2}{8\pi^2\alpha_1^8}F_a^2\left(\frac{\omega}{2}\right)\int_0^{u_{\max}}|E_p|^2 \times\left[\int_0^{2\pi}|\Gamma_v(u,\theta_k,\mathbf{r})|^2 \times I^{(2)}(u,\theta_k,\omega)\,d\theta_k\right]u\,du, \qquad (11)$$

where

$$\Gamma_v(u,\theta_k,r)=\int_s\hat{G}_v(\mathbf{r},\mathbf{r}_0)e^{i\mathbf{k}\mathbf{r}_0}d\mathbf{r}_0\,, \qquad (12)$$

$$\hat{G}_v(\mathbf{r},\mathbf{r}_0)=\int_0^\infty ff_v(u')J_0(\xi u')u'\,du', \qquad (13)$$

$$ff_v(u')=\frac{1-R_b}{1+R_b}\sqrt{1-u'^2}\,. \qquad (14)$$

In the numerical integration of Eq. (11), the upper limit of the relative wave number, $u_{\max}$, can assume different values depending on the nature of the problem. For instance if the water layer is so deep that the factor $e^{i2k_1'h_1}$ suppresses all contributions from components of $u>1$ we can take $u_{\max}=1$, as is done traditionally in the literature. Since the integrand for $u>1$ has an approximate form of $u^3e^{-2(\omega h_1/\alpha_1)u}$, in the general case a value of three times the corner value, i.e., $u_{\max}=3u_m=4.5\alpha_1/\omega h_1$, can be used as a reasonable upper limit in the numerical calculations. In any event, $u_{\max}$ is bounded by an extreme value of $\omega\alpha_1/g$ for second-order wave interactions.[12] This finite limit to the horizontal wave number and the generally nonwhite nature of the factor $I^{(2)}(u,\theta_k,\omega)$ are two notable features of the source of the wave-generated noise field. It therefore has a finite spatial correlation distance at the surface of the order of the wave length of the interacting gravity waves.

The spectrum of the pressure field at depth z thus takes the form

$$F_p^{(2)}(\omega,z)=\frac{1}{2}\frac{\omega^3}{\alpha_1^2}\rho_1^2g^2F_a^2\left(\frac{\omega}{2}\right)\int_0^{u_{\max}}|E_p|^2\bar{I}(u,\omega)u\,du, \qquad (15)$$

where

$$\bar{I}(u,\omega)=\int_0^{2\pi}I^{(2)}(u,\theta_k,\omega)d\theta_k, \quad E_p=E_p(\omega,u,z).$$

II. THE SEISMOACOUSTIC SPECTRUM INSIDE AN ACTIVE REGION OF INFINITE SIZE

We now consider the seismic response from an active region of infinite size as a special case. (This case was discussed briefly in Refs. 8 and 9.) We first see that the operations in Eqs. (12) and (13) can be cancelled by using the property[16]

$$\sqrt{ab}\int_0^\infty J_m(a\chi)J_m(b\chi)\chi\,d\chi=\delta(a-b)$$

whereupon the seismic spectrum, Eq. (11), degenerates to

$$F_{mv}^{(2)}(\omega)=\frac{\omega g^2}{2\alpha_1^4}F_a^2\left(\frac{\omega}{2}\right)\int_0^{u_{\max}}|E_v|^2\bar{I}(u,\omega)|1-u^2|u\,du, \qquad (16)$$

where

$$E_v=\frac{1-R_b}{1+R_be^{i2k_1'h_1}}e^{ik_1'h_1}. \qquad (17)$$

As we discussed in Refs. 8 and 9, a set of spectral transfer functions can be defined to convert spectra from one field to the other. As an example, the transfer function $T_{mp}(\omega)$ relating the seismic response and the pressure field can be defined as the ratio of the measured microseismic spectrum to the source pressure spectrum. The pressure spectrum defined by Eq. (15), however, is the spectrum of the total pressure field including as it does both homogeneous and inhomogeneous components. To be consistent with the widely used definition of the surface-noise source level,[17] corresponding to the radiating part of the surface noise source, we introduce the simplified source pressure spectrum of the wave-interaction process by taking $u_{\max}=1$ and $\chi=1$, $\hat{m}=\hat{t}=0$ in $I^{(2)}(u,\theta_k,\omega)$, to obtain:

$$F_{pr}^{(2)}(\omega)=\frac{\pi}{2}\frac{\omega^3}{\alpha_1^2}\rho_1^2g^2F_a^2\left(\frac{\omega}{2}\right)I(\omega), \qquad (18)$$

where

$$I(\omega)\equiv\int_0^{2\pi}H(\theta-\theta_\omega)H(\theta+\pi-\theta_\omega)d\theta$$

and θ_ω is the wind direction.

In this case the ratio of Eqs. (16) and (18) ($\equiv T_{mp}^{-1}$),

$$T_{pm}(\omega)=\frac{1}{\pi I(\omega)\rho_1^2\omega^2\alpha_1^2}\int_0^{u_{\max}}|E_v|^2\bar{I}(u,\omega)|1-u^2|u\,du \qquad (19)$$

and that of Eqs. (15) and (18)

$$T_{pp}(\omega)=\frac{1}{\pi I(\omega)}\int_0^{u_{\max}}|E_p|^2\bar{I}(u,\omega)u\,du \qquad (20)$$

define respectively the microseismic and pressure spectra produced by a radiating noise source of unit level.

The function $\bar{I}(u,\omega)$ is generally not constant in either the frequency or wavenumber domain. It is also wind dependent as is shown by a comparison of Fig. 1(a) (wind speed 30 m s^{-1}) and Fig. 1(b) (10 m s^{-1}). The decrease in the magnitude of the function at low frequencies and

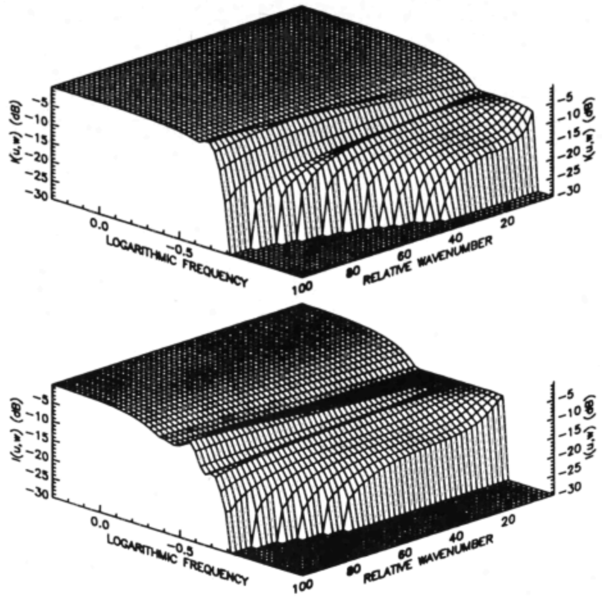

(a)

(b)

FIG. 1. A plot of the term $I(u,\omega)$ as a function of logarithmic frequency and relative wave number: (a) for wind speed 30 m s^{-1} and (b) wind speed 10 m s^{-1}.

high wave numbers results from the reduction in nonlinear wave interaction activity. By virtue of the nature of this process there is an upper limit to u at any frequency. This value corresponds to the value below which the cubic equation in χ has a single real root.[12] For computational reasons it is here set at $u=0.96\omega\alpha_1/2g$. In Fig. 1(a) this upper limit corresponds to the intersection of the function $\bar{I}(u,\omega)$ with the -30-dB plane. In Fig. 1 it is shown only for values of u less than 100, but the intersection curve continues to higher wave numbers and frequencies. The sharp drop in the function at low frequencies is caused by the steep drop which characterizes the ocean-wave spectrum at frequencies below the peak. As expected, at the lower wind speed this scarp occurs at higher frequencies—Fig. 1(b). At high frequencies and low relative wave numbers the function tends to be much flatter in form, the fluctuations in level being less than 10 dB. As in other parts of the paper the JONSWAP form of the wave spectrum has been used in the calculation.

The wave-number dependence of $\bar{I}(u,\omega)$ makes it difficult to separate source effects (wind speed) from the medium response (E_v and E_p). However if the low-frequency limit is not allowed to fall much below the peak frequency of the pressure field we can set $\bar{I}(u,\omega)\simeq 2\pi I(\omega)$ and bring this term outside of the integral to leave the transfer functions independent of the characteristics of the source. With this approximation Eqs. (19) and (20) become

$$T_{pm}(\omega)\approx\frac{2}{\rho_1^2\omega^2\alpha_1^2}\int_0^{u_{\max}} |E_v|^2|1-u^2|u\,du \qquad (21)$$

and

$$T_{pp}(\omega)\approx 2\int_0^{u_{\max}} |E_p|^2 u\,du. \qquad (22)$$

TABLE I. Parameters of the geoacoustic models.

n	Density ρ_n kg m^{-3}	Thickness h_n m	Comp. Vel. (m/s) α_n	Shear Vel. (m/s) MDK1	MDK2	Q values Q_{an}	Q_{bn}
1	1000	100	1500	···	···	···	···
2	1700	400	1560	···	···	10	···
3	1900	850	2000	700	1154	500	300
4	2300	1675	3100	1000	1789	500	300
5	2500	1775	4100	1500	2367	500	300
6	2500	···	5000	2500	2885	500	300

Apart from the factor $1/\rho_1^2\omega^2\alpha_1^2$ and the finite integration limit, Eq. (21) is equivalent to Eq. (5) in Schmidt and Kuperman's paper.[10] This will be relevant later.

III. NUMERICAL CALCULATIONS

To demonstrate the characteristics of these functions we use the six-layered model which we have taken as representative of the geoacoustical environment where the New Zealand spectra were recorded. For the sake of comparison we use two variants of this model, MDK1 and MDK2, differing only in the shear-wave velocities of each layer. In MDK1 these are at the lower end of the accepted range and the same as those used by Schmidt and Kuperman in their analysis of this model;[10] in MDK2 the shear-wave velocities are at the higher end of the accepted range and assigned according to the formula $\beta_n=\alpha_n/\sqrt{3}$. The values of the parameters used in the two models are shown in Table I.

Schmidt[18] has recently provided a useful review of the numerical models now available for the study of wave propagation in horizontally stratified viscoelastic media. The care which has to be exercised in developing such codes is well documented in this review and in his paper with Jensen describing one of the more recently developed techniques.[19] Because of the complexities involved certain models such as SAFARI have become bench marks against which the performance of new codes are evaluated.[20] The codes we have developed to carry out the studies described below have been validated by demonstrating that they reproduce faithfully the results reported in Ref. 19 and, of particular relevance to this paper, those in Ref. 10.

The reflection loss ($-20\log_{10}R_b$) calculated for the two versions of the New Zealand model is presented as the bottom of the three plots in Fig. 2 (MDK1) and Fig. 3 (MDK2). The other two plots in these figures represent the reflection loss for two simplified versions of these models, MD1(1), MD1(2), MD2(1), and MD2(2). In MD1(1) the water layer overlies a solid half-space with the properties of the basement in MDK1, while in MD1(2) the water layer overlies a half-space with the properties of the basement in MDK2. MD2(1) and MD2(2) are the same (but are reproduced for convenience in both figures). In both the water layer overlies an unconsolidated-half space (both will be denoted as MD2 below).

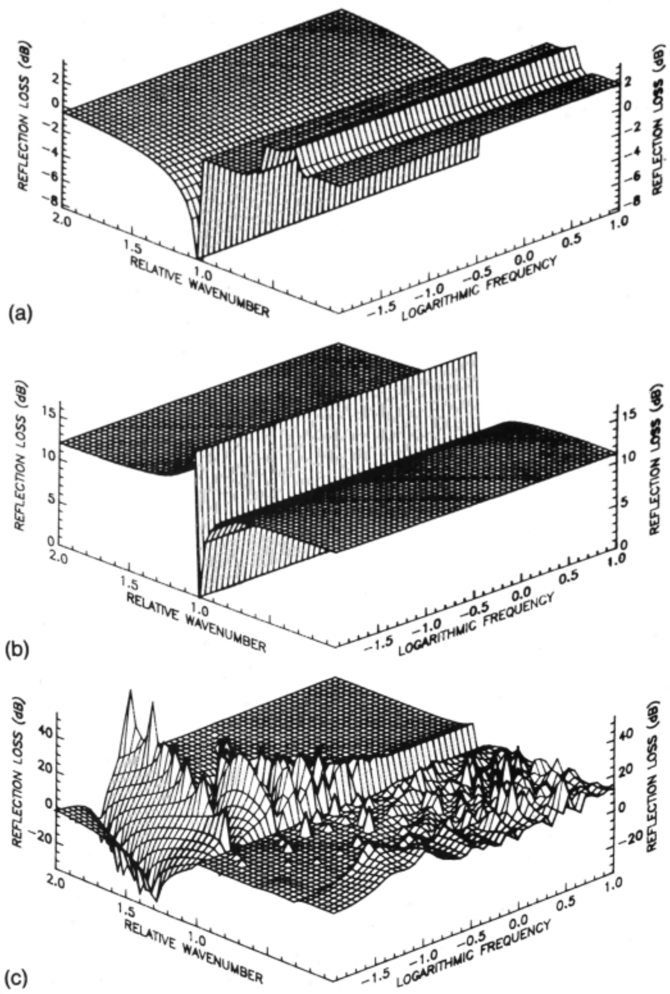

FIG. 2. Reflection loss for three typical ocean models using shear-wave speeds based on MDK1: (a) solid half-space; (b) an unconsolidated half-space; (c) a multilayered half-space.

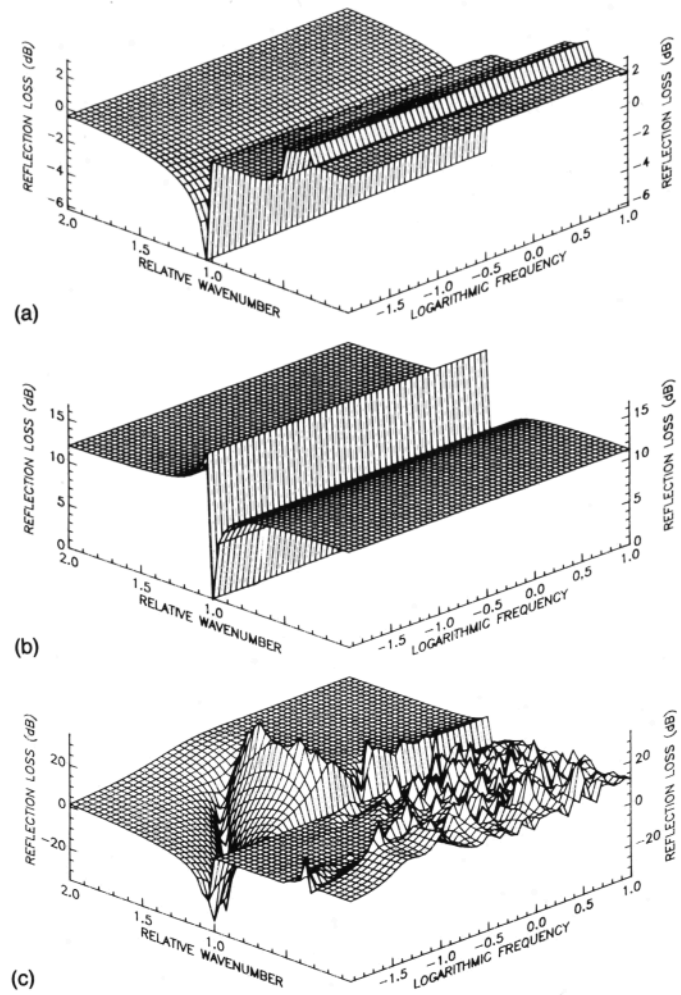

FIG. 3. Reflection loss for the models depicted in Fig. 2 but with shear-wave speeds based on MDK2.

From these plots it is clear that in the case of MDK2 most of the structure in the reflection loss is restricted to the region $0 \leqslant u \leqslant 2$. In contrast, in MDK1 the structure extends through the range $0 \leqslant u \leqslant 3$ (although the plot is restricted to $0 \leqslant u \leqslant 2$). The explanation for this structure in terms of the model parameters proves to be very interesting,[21] but in the interests of brevity a full discussion of this subject is deferred to a later paper. We simply point out here that the bottom properties which produce the main characteristics of the reflection loss behavior can be well identified in the pictures shown in Figs 2 and 3.

The integrals of the functions $|E_v|^2$ and $|E_p|^2$ for the models MDK1 and MDK2 are plotted as functions of the relative wave number, u, and frequency, in Figs. 4 and 5. The peaky nature of the functions clearly emphasises the need to use very small increments at low values of u (say $u \leqslant 3$) in the numerical integration of the transfer and spectral functions. To emphasize this point we select from Figs. 4 and 5 the profile corresponding to the frequency 0.22 Hz [a value close to double the peak frequency of the JONSWAP form of the wave spectrum in the New Zealand environment at a wind speed of 30 m s^{-1} (Ref. 22)] and in Figs. 6 and 7 present this profile as a function of u for models MD1(1), MD2, MDK1, and MDK2—over the range $0 < u \leqslant 3$ in Fig. 6 and over the range $3 < u \leqslant 100$ in Fig. 7. The dependence of the microseism spectral levels (for the same models) on the sampling interval used in the calculations over the range $0 < u \leqslant 3$ is demonstrated in Fig. 8. For each of the models, the three spectral levels shown, corresponding to the cases $u \leqslant 1$, 3, and 100, demonstrate the relative importance of the different wave-number components. In the case of model MD1(1), for instance, the inhomogeneous component ($u > 1$) contributes little to the total level, as is to be expected from the corresponding plots in Figs. 6 and 7. In contrast, in the model with the unconsolidated half-space (MD2), the inhomogeneous component can lift the spectral levels as much as 40 dB above those arising from the homogeneous component alone. In the case of MDK1 the inhomogeneous contribution is again large (25 dB), reflecting the fact that most of the surface wave modes have horizontal wave numbers greater than ω/α_1. This contribution drops to about 10 dB (at sufficient integration accuracy) in MDK2, reflecting in turn the higher bottom rigidity characterizing this model.

These figures show that inside the active region the bottom response to a source pressure component of unit

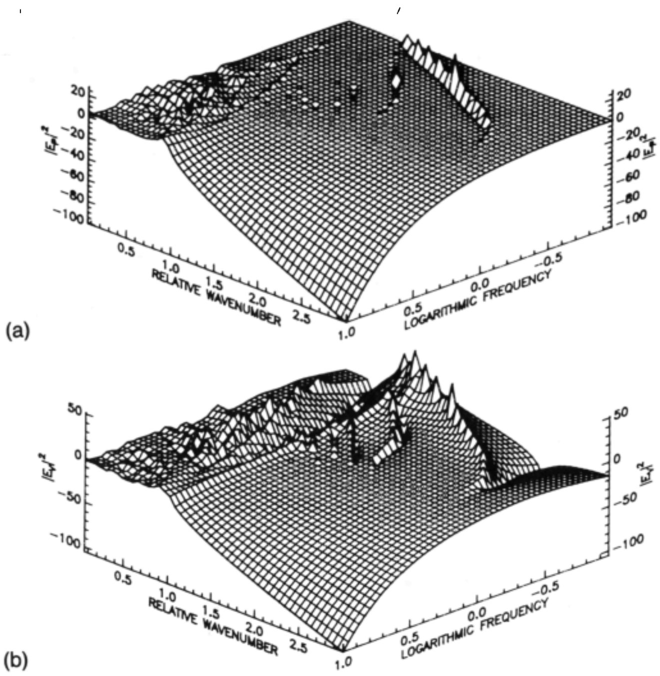

FIG. 4. The functions $|E_p(u,\omega)|^2$ and $|E_v(u,\omega)|^2$ for a bottom structure with low shear-wave speeds (model MDK1).

level at this frequency, depends critically on the geoacoustic model, and particularly on the presence or absence of an upper unconsolidated layer associated with an adjacent layer of low shear-wave velocity. Also obvious is the importance of the sampling interval used at low wave numbers in the numerical calculations. To ensure a reasonable accuracy for $u \leqslant 3$ a value of $\delta u = 0.002$ has been used in all later calculations to be described below. This resolution

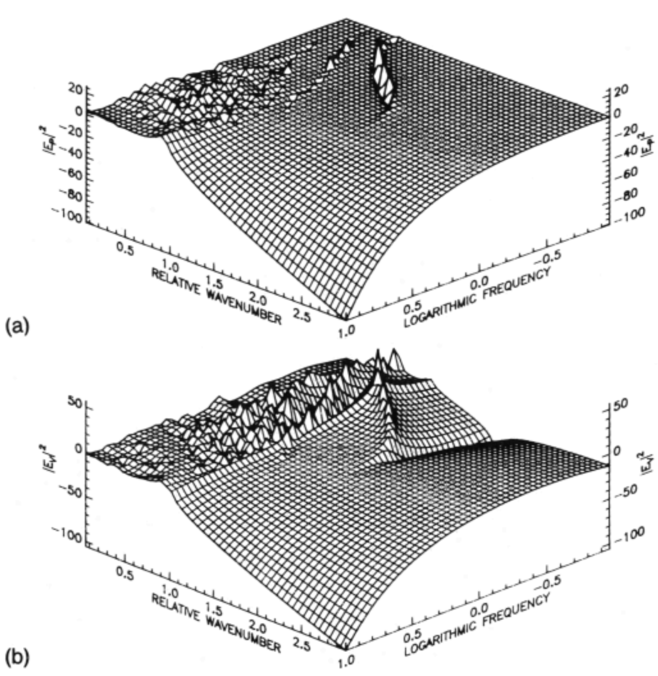

FIG. 5. The functions $|E_p(u,\omega)|^2$ and $|E_v(u,\omega)|^2$ for a bottom structure with high shear-wave speeds (model MDK2).

provides a reasonable compromise between accuracy and computation costs.

Figure 9 presents the transfer function, $T_{pp}(\omega)$, relating the source pressure spectrum to the ULF pressure spectrum expected near the bottom (in this case 100 m below the sea surface), for the two models MDK1 and MDK2. Curves 1, 2, and 3 represent, respectively, the contributions of all wave number components up to $u \leqslant 100$, $u \leqslant 3$ and $u \leqslant 1$. Figure 10 shows the same plots for the function $T_{pm}(\omega)$. The upper limit of the integration has been set at $u_{\max} = \omega\alpha_1/g$ if the value of $\omega\alpha_1/g$ is less than 100 and at $u_{\max} = 100$ if it is greater than 100.

The plots in Figs. 9 and 10 show the relative importance of the inhomogeneous component as a function of frequency. Figure 11, on the other hand, shows the variation of the transfer function, $T_{pm}(\omega)$, with model type. Curve (1) shows the behavior of T_{pm} for the solid bottom models MD1 (1) and (2); curve 3 for the six-layered models MDK1 and MDK2; and curve (4) for the six-layered structure when the top unconsolidated layer is absent. Of immediate note is the role played by the unconsolidated layer in determining the behavior of the total transfer function. In its absence the transfer function is suppressed at low frequencies, enhanced at high frequencies and modulated by the deeper layers. In the environment of the New Zealand experiment in particular, the upper unconsolidated sediment of 400-m thickness appears to effectively mask the influence of all substructure on the pressure and seismic fields for an active region on the continental shelf ($h_1 \sim 100$ m). In this case the seismic response can apparently be evaluated adequately by representing the seabed as a liquid half-space—see curve (2). At very low frequencies the unconsolidated layer becomes "thin" and the inhomogeneous component can have significant levels at much greater depths. In this situation deeper structures, not represented in the present models, will have an important influence on the transfer function. A more complete evaluation of such effects based on earth models incorporating deeper structures will be included in a paper in preparation.

It is also of interest that in both model MDK1 and MDK2, the transfer function displays a sharp peak at a very low frequency around 0.05 Hz. This peak is more clearly seen in Fig. 12 where a logarithmic frequency scale is used. Figure 13 shows the sensitivity of the whole transfer function, and this peak, to an increase in the thickness of the water layer from 100 to 500 to 1000 m. The high peak is caused by the combined effects of the upper limit of the horizontal wave number, $k_{\max} = \omega^2/g$, and the exponential decay embodied in the factor $e^{-2u\omega h_1/\alpha_1}$ in the integrand $|E_v|^2$ (or $|E_p|^2$) of Eq. (19). As a rough estimate of the transfer function in the low-frequency region we can write Eq. (19) as the sum

$$T_{pm}(\omega) = T_{pm1}(\omega) + T_{pm2}(\omega),$$

where

$$T_{pm1}(\omega) = \frac{2}{\rho_1^2\omega^2\alpha_1^2}\int_0^1 \left|\frac{1-R_b}{1+R_b e^{ik_1' h_1}}\right|^2 (1-u^2)u\,du$$

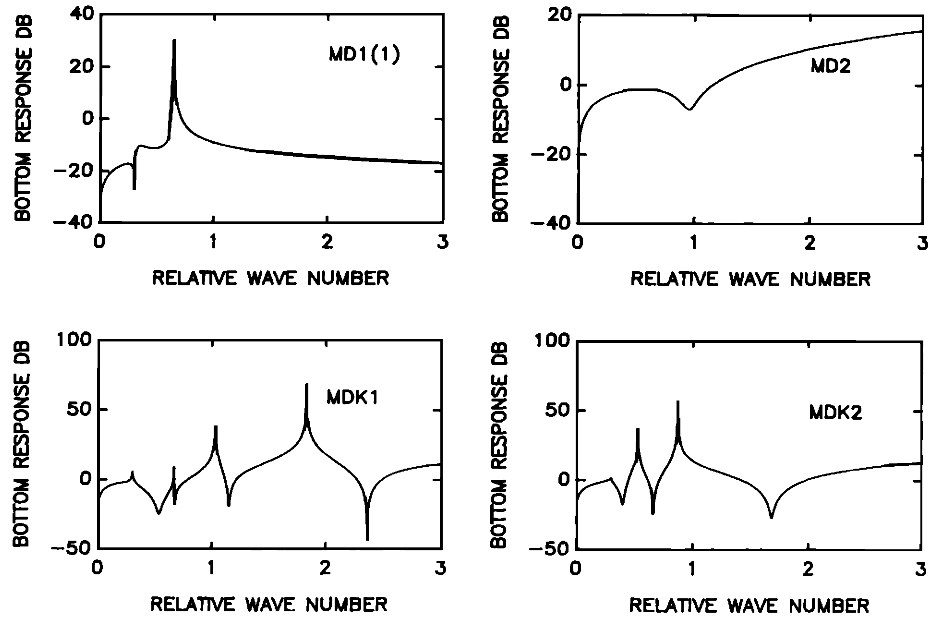

FIG. 6. The bottom response at the frequency 0.22 Hz for the models MD1, MD2, MDK1, and MDK2 described in the text, as a function of relative wave number $0 \leqslant u < 3$.

and

$$T_{pm2}(\omega) = \frac{2}{\rho_1^2 \omega^2 \alpha_1^2} \int_1^{\omega\alpha_1/g} \left| \frac{1-R_b}{1+R_b e^{-\sqrt{u^2-1}\,\omega h_1/\alpha_1}} \right|^2 \times e^{-2(\omega h_1/\alpha_1)\sqrt{u^2-1}} (u^2-1) u \, du$$

(at higher frequencies, if $\omega\alpha_1/g > 100$, $u_{\max}=100$ as mentioned earlier). In shallow water environments with an unconsolidated layer of finite thickness, the term T_{pm2} is roughly proportional to

$$T_{pm2}(\omega) \approx \frac{2A}{\rho_1^2 \omega^2 \alpha_1^2} \int_1^{\omega\alpha_1/g} e^{-2\omega h_1 u/\alpha_1} (u^2-1) u \, du.$$

Evaluating $\partial T_{pm}/\partial\omega = 0$ we establish that the peak in the transfer function will occur around $f_m = (0.4/\pi)\sqrt{g/h_1}$, so that the small decrease in f_m with increasing water depth h_1, shown in Fig. 13, is to be expected.

Figure 14 presents the transfer functions for two other simplified (but idealized) models, one involving shallow and the other deep waters. Each model is characterized by a solid basement with $\alpha_3 = 5000$ m s^{-1}, $\beta_3 = 2500$ m s^{-1},

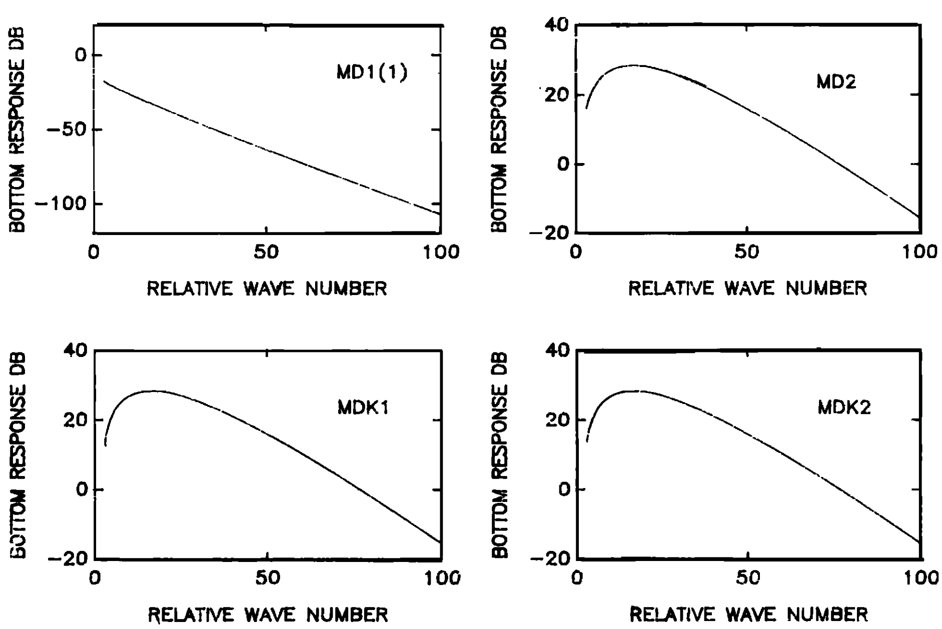

FIG. 7. The bottom response at the frequency 0.22 Hz for the models MD1, MD2, MDK1, and MDK2 described in the text, as a function of relative wave number $3 \leqslant u < 100$.

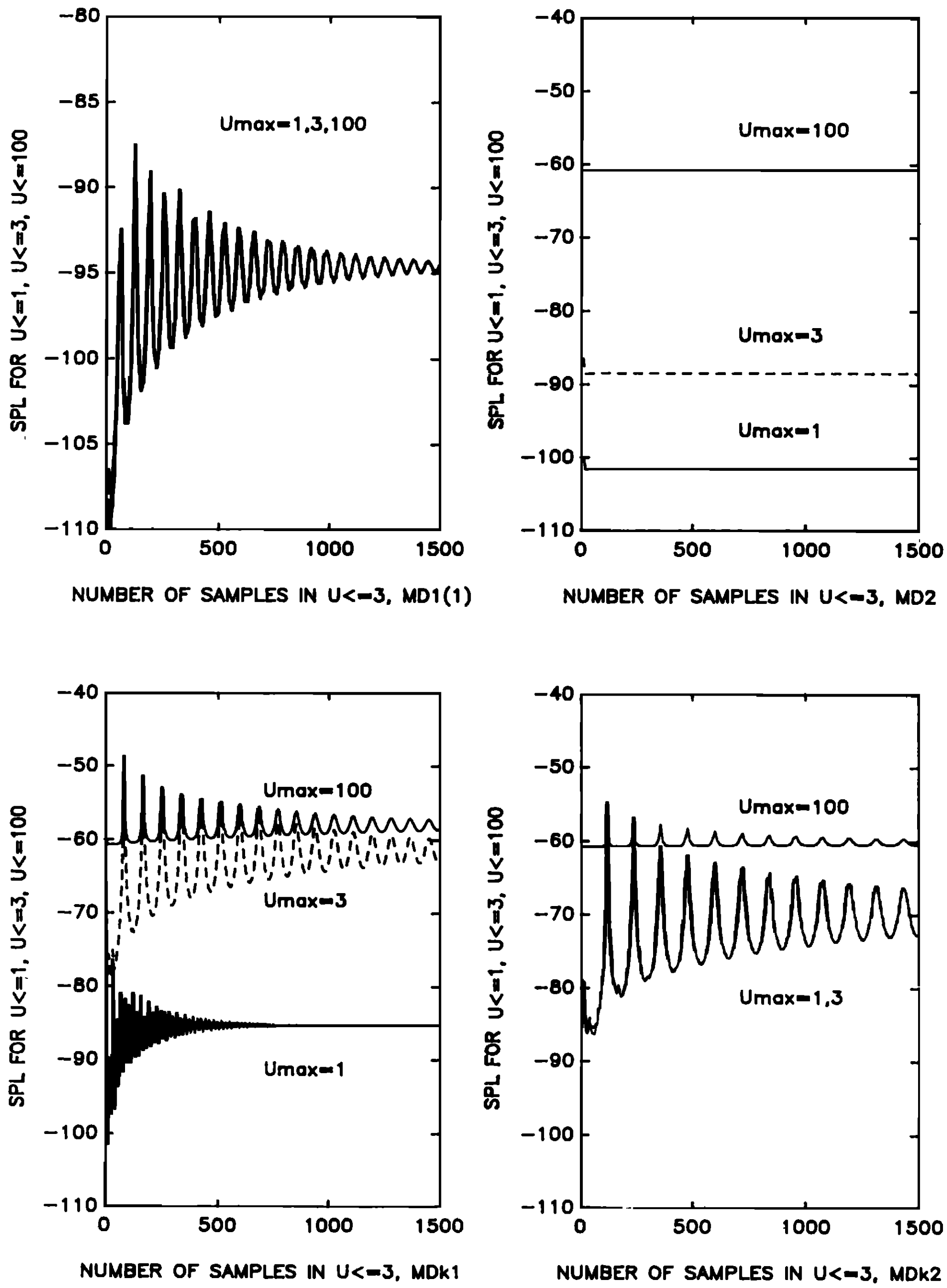

FIG. 8. A demonstration of the influence of the sampling rate on the numerical accuracy achieved with different models—frequency 0.22 Hz, relative wave number $0<u<3$.

and an unconsolidated middle layer of thickness $0 \leqslant h_2 \leqslant 1000$ m, with $\alpha_2 = 1560$ m s^{-1} and $Q_{\alpha 2} = 10$. The water depths are, respectively, 100 m (shallow) and 4000 m (deep). The different curves show the variation of the transfer function with the thickness of the unconsolidated layer, $h_2 = 0$, 50, 100, 200, 500, and 1000 m. [To show the variation with h_2 in more detail, three more thicknesses, $h_2 = 5$, 10, and 20 m, are plotted in Fig. 14(a).] It is seen that in the shallow-water case significant changes occur at small values of h_2 (from 0–50), that the transfer function stabilizes at higher values of h_2, and that the peak frequency follows the relationship given above. In the case of the deep ocean, on the other hand, the seismic response is proportional to the thickness h_2 for frequencies less than 0.07 Hz, but inversely proportional to the thickness above this frequency. We will discuss the significance of this behavior to the ULF spectrum below 0.05 Hz in a later paper.

IV. THE GREEN'S FUNCTIONS

Having discussed the special case of an active region of infinite size, we now examine how the microseismic response to wave–wave interaction varies as the observation point is moved from the center of to outside an active region of finite size. As a first step we calculate the required Green's functions, according to Eq. (13), for the models discussed above. Although straightforward, the calculation

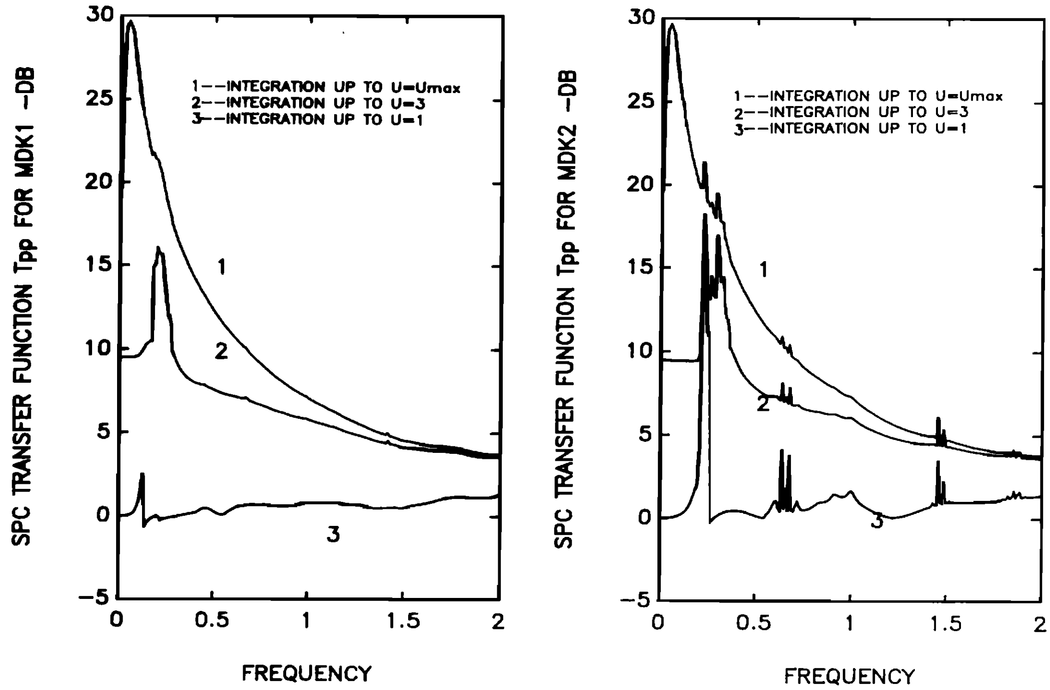

FIG. 9. Plots demonstrating the influence of the inhomogeneous component on the pressure-pressure transfer function for the multilayered models MDK1 and MDK2.

can be very complicated in some cases. For example, when the top layer of the bottom structure is an unconsolidated medium R_b tends to a constant value (less than one) when kh_2 is much greater than one and the integration of Eq. (13) may not converge. Actually in the ideal case of a model involving two liquid layers no poles exist in the wave-number plane and the Green's function takes the characteristic of a δ function in space. This behavior, in turn, makes the calculation of $\Gamma_v(u,\theta_k)$ critically dependent on the size of the grid used and the position of the observation point relative to the grid. If, in this case, the size of the grid is chosen too small, the calculated value for the point $\mathbf{r}$ nearest to the source point $\mathbf{r}_0$ can become very large. To make the calculation numerically proper, it is

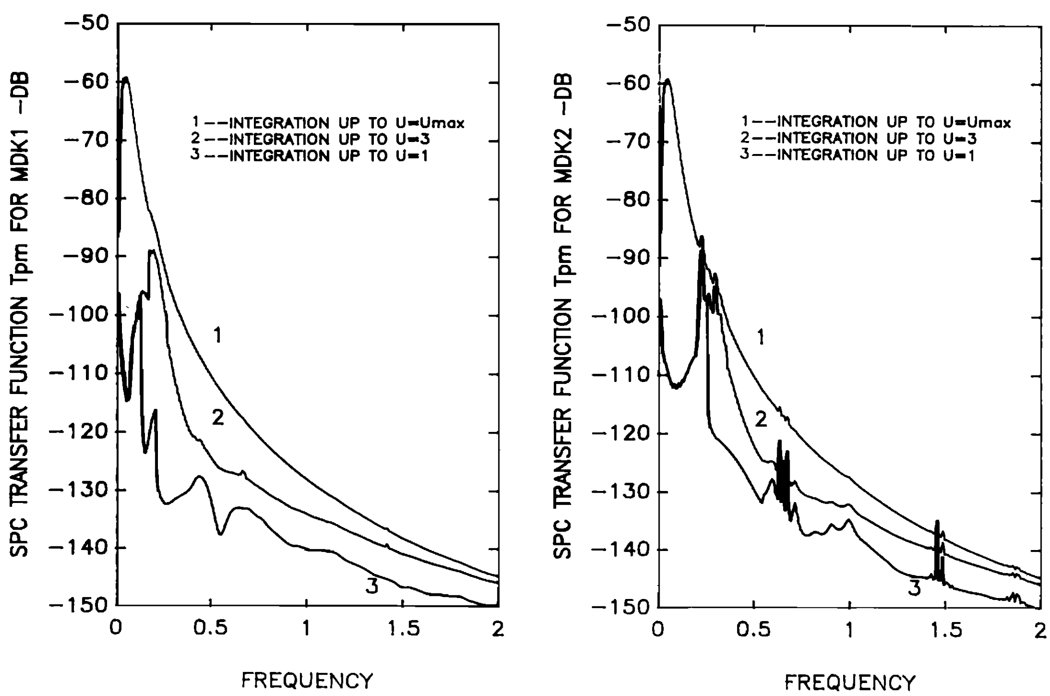

FIG. 10. Plots demonstrating the influence of the inhomogeneous component on the pressure-ground displacement transfer function for the multilayered models MDK1 and MDK2.

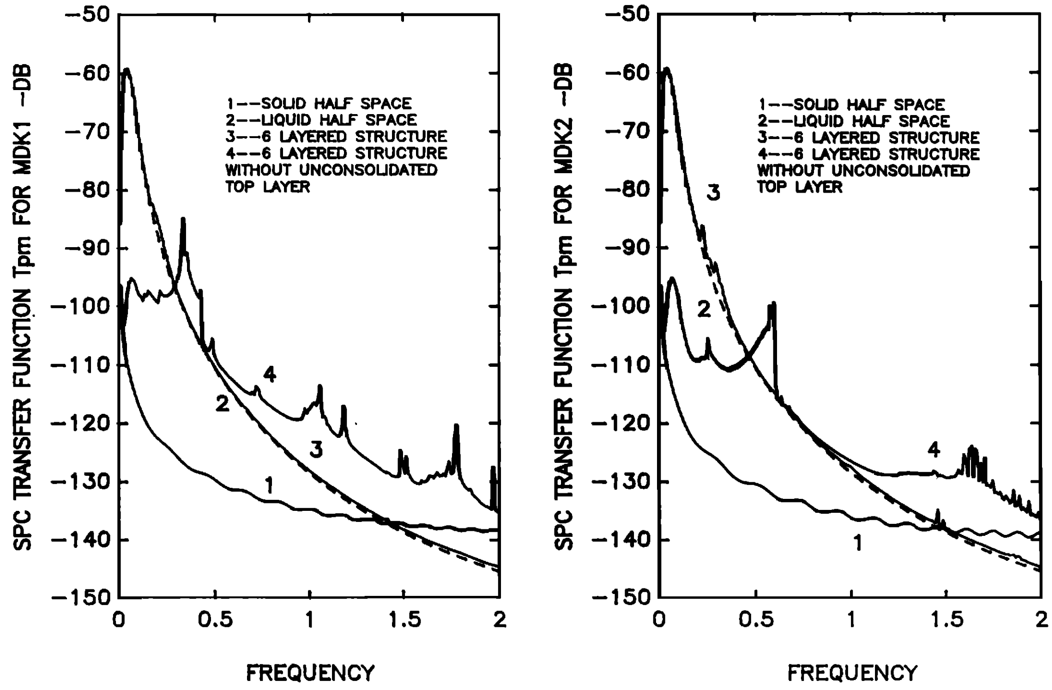

FIG. 11. Plots demonstrating the dependence of the pressure-ground displacement transfer function (linear frequency scale) on the bottom structure.

necessary to set an upper limit to the relative wavenumber u'_{max} in Eq. (13). A reasonable approximation is to take u'_{max} equal to the physical upper limit $u_{\max}$ used in Eq. (11). The size of the spatial grid used in the 2D-FFT processing of Eq. (12) can be related to $u'_{\max}$ through the Nyquist theorem. While this truncation introduces a certain error into the calculation, it can be shown that this error decreases with increasing size of the active region when the observation point is inside it, and quickly reduces with distance for observation points outside the region—see Appendix A.

Figures 15 to 18 present the amplitude of the Green's functions for the models MD1(1), MD1(2), MD2, MDK1, and MDK2, calculated over the range interval 0.01 to 30 km. Several features can be noticed: (i) In the case of the solid-bottom models [MD1(1) and MD1(2)]

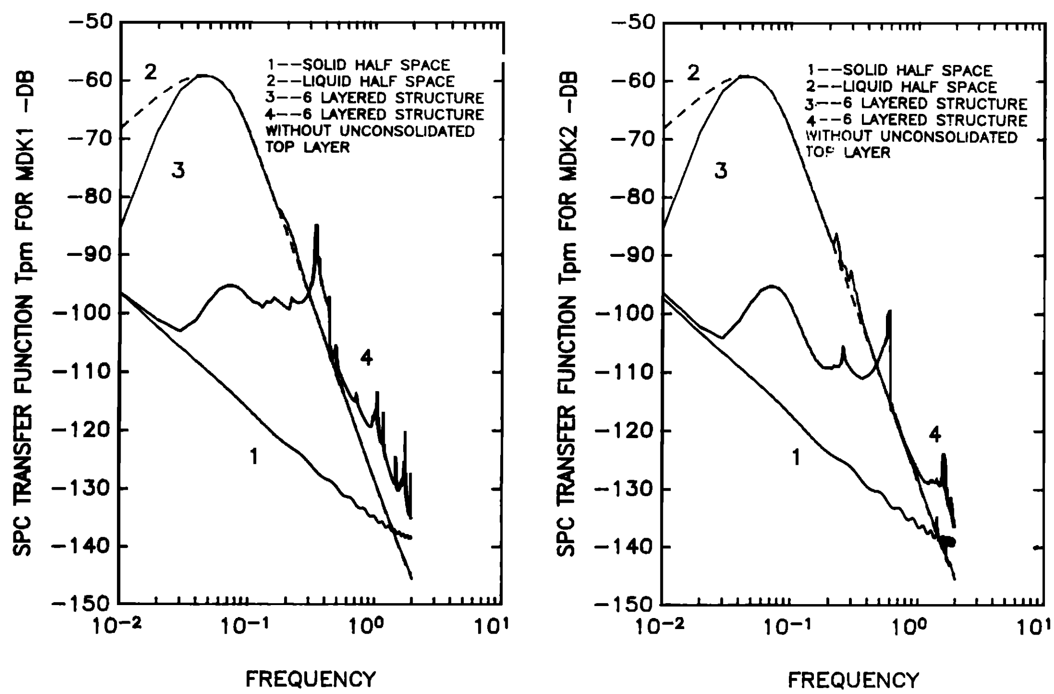

FIG. 12. Plots demonstrating the dependence of the pressure-ground displacement transfer function (logarithmic frequency scale) on the bottom structure.

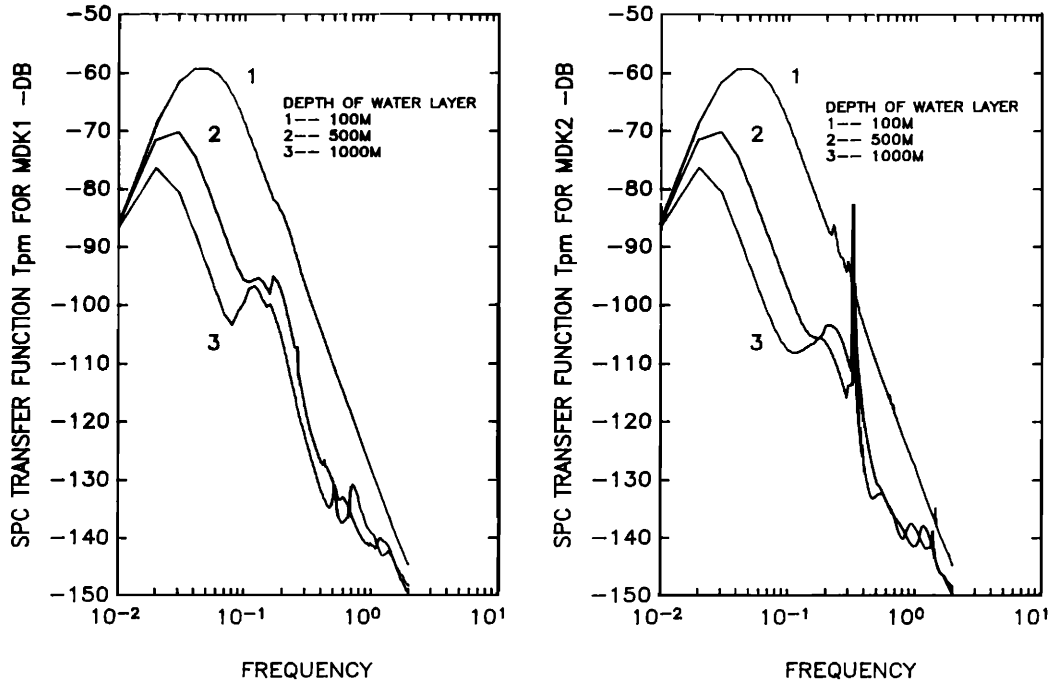

FIG. 13. Plots demonstrating the influence of the water depth on the pressure-ground displacement transfer function in multilayered environments.

the curve for MD1(2) is some 20 dB higher than that for MD1(1) (see Fig. 15) and the maximum value of the Green's function in both is much lower (down by around 70 dB) than those in the other models—Figs. 16–18. This is simply because, in the case of a hard bottom, the reflection coefficient R_b is very close to unity for $u' > 1$, and the inhomogeneous component of the seismic displacement cannot be excited strongly. (ii) The oscillations apparent in Fig. 15 at short ranges are the result of the wave-number truncation. The average distance between peaks, L, estimated from Fig. 15, is about 135 m, a value which approximates the wavelength $\lambda = 2\pi\alpha_1/(u_{\max}\cdot\omega) \cong 140$ m corresponding to the value $u_{\max}$ ($=48.2$) used. The oscillations in the far field, on the other hand, can be recognized as a manifestation of the Rayleigh wave, which has a wavelength of about 10 km at 0.22 Hz. (iii) Figure 16 shows

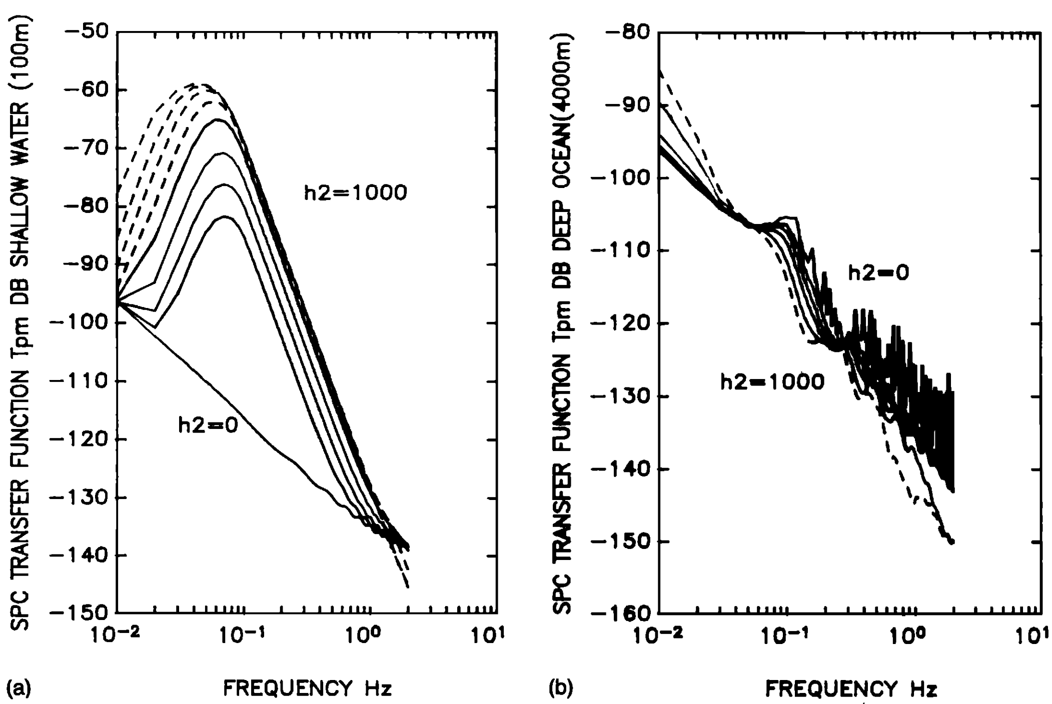

FIG. 14. Plots demonstrating the influence of the thickness of the unconsolidated sedimentary layer on the pressure-ground displacement transfer function for a three-layered ocean model: (a) shallow water; (b) deep ocean.

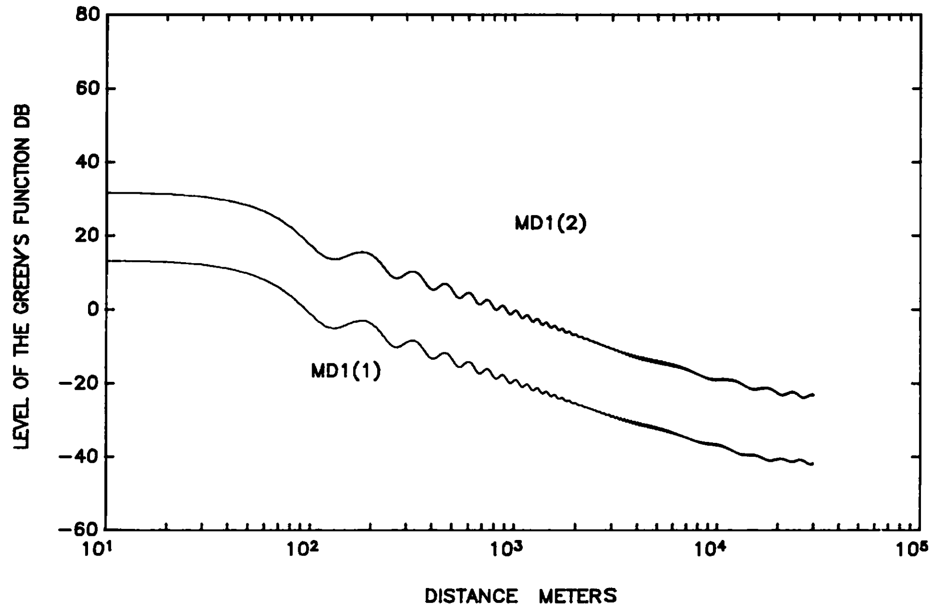

FIG. 15. The amplitude of the Green's function as a function of range for model MD1—a solid half-space.

that the Green's function for MD2 has a high level near the source point. This is a consequence of the fact that R_b takes a nonzero finite value (about 0.37) at large u', for reflection from the unconsolidated half-space. The oscillations in the near field again result from the truncation of the wave-number axis. In the far field the large negative logarithmic values are thought to correspond to the zeros of the lateral wave propagating along the interface.[23] Since there are no poles in the case of two contacting liquid half-spaces, no acoustic interface wave mode will be excited. As a consequence the Green's function decays with distance much faster than is the case for the solid bottom—see Fig. 15. (iv) While Figs. 17 and 18 show the Green's functions are more complicated in the multilayered case, the near-field characteristics are seen to be similar to those of the simplified model, MD2, involving an unconsolidated half-space (Fig. 16). This is to be expected since in a shallow-water environment the seismic field at large horizontal wave numbers is determined mainly by the properties of the top sedimentary layer. (v) Finally, the Green's functions for the two multilayer models (MDK1 and MDK2) differ from each other in the far field because of the effects of interface wave modes. In the case of MDK2 (Fig. 18) the shear-wave velocities of each sublayer are high (compared with those of MDK1), and most interface wave modes have horizontal wave speeds close to that of the basic Rayleigh wave mode. In the case of MDK1, on the other hand, the interface wave velocities are more widely

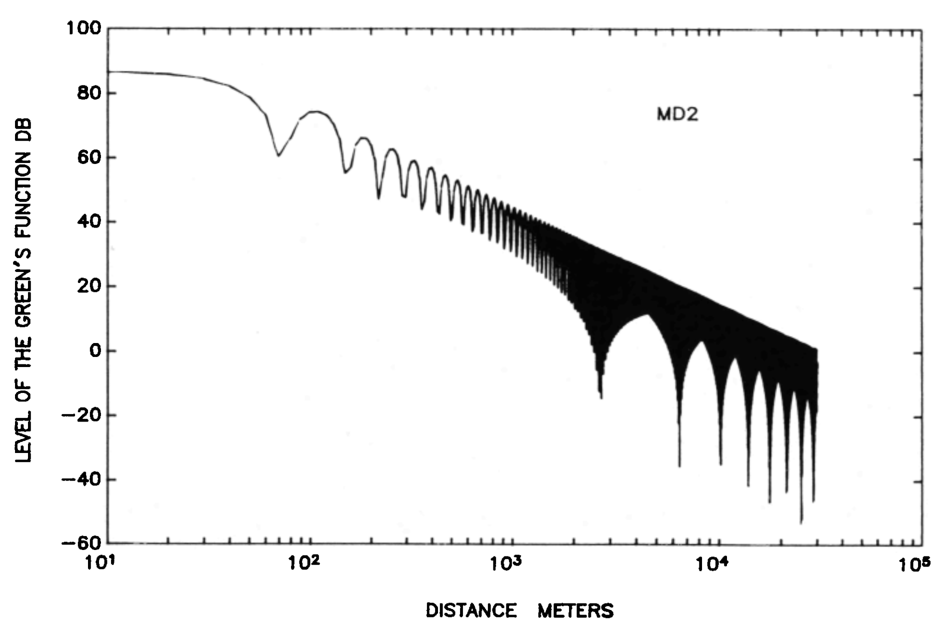

FIG. 16. The amplitude of the Green's function as a function of range for model MD2—an unconsolidated half-space.

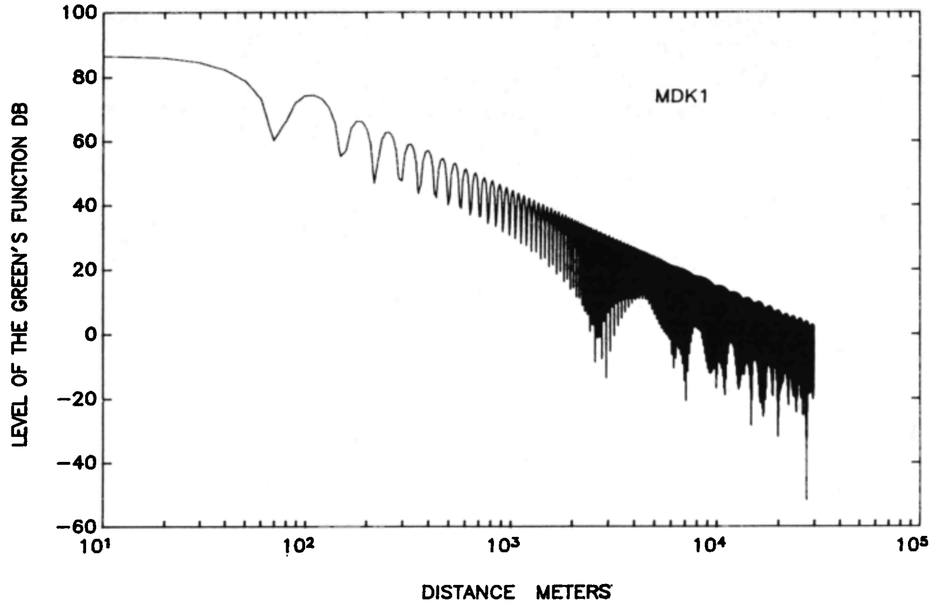

FIG. 17. The amplitude of the Green's function as a function of range for the multilayered model (MDK1) with low shear-wave velocities.

distributed and, as is shown in Fig. 17, the interference effects become more complicated.

While Figs. 15–18 are restricted to a range of 30 km the Green's functions for the three models were calculated out to 10^6 m in steps of 10 m to meet the requirements of the far-field calculations, which are discussed in the next section.

V. THE SEISMIC RESPONSE OUTSIDE AN ACTIVE REGION

Using the Green's functions discussed in the last section, it becomes a straightforward matter to establish the microseismic response as a function of the distance from the center of the active region. The size of the active wave region used in the numerical calculation, 80×80 km^2, was chosen as a compromise between computation cost and the dimension necessary to demonstrate clearly the main characteristics of the wave-induced seismic response in the transition region. It can be shown, however, that all the characteristics demonstrated below become even more pronounced when the size of the active region is further increased.

We first examine the simplest model, MD2, with the unconsolidated (liquid) bottom. The decay of spectral level (at 0.22 Hz) with distance from the center of an active area of finite size is shown by curve (1) in Fig. 19. In this figure the horizontal lines (2) and (3) indicate respectively the seismic response to the total pressure field (in-

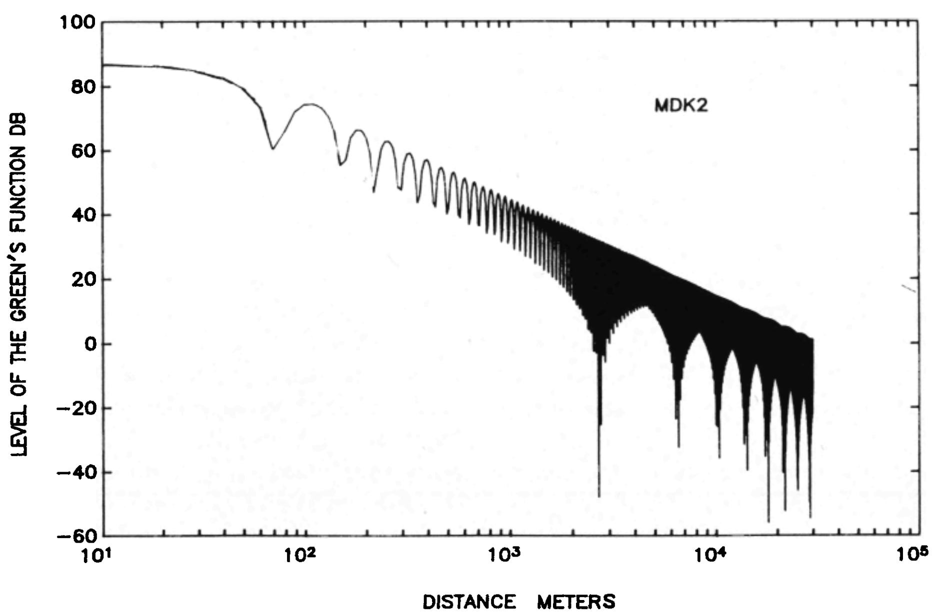

FIG. 18. The amplitude of the Green's function as a function of range for the multilayered model (MDK2) with high shear-wave velocities.

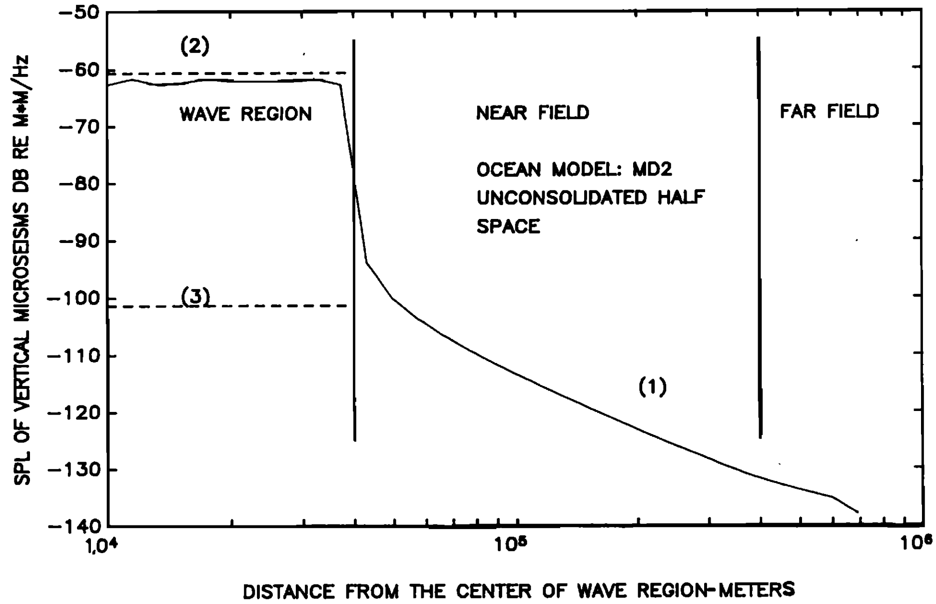

FIG. 19. Decay of the vertical seismic spectral level with distance from the center of the active wave region, above an unconsolidated bottom.

cluding both the inhomogeneous and homogeneous components) when the active region is infinite in size (using the high sampling rate described in the last section) and that to the homogeneous component alone. A wind speed of 30 m s^{-1} and the JONSWAP form of the ocean-wave field are assumed. The plot simply confirms that, for this model, the inhomogeneous component dominates the seismic response inside the active region. However the plot also demonstrates that the influence of the inhomogeneous component reduces rapidly as the sensor is moved beyond the bounds of the active region. Just outside the active region the seismic response arises primarily from the diffracted field associated with the homogeneous component of the pressure field. Since the wavelength of this component ($\sim$7 km) is comparatively large compared with the size of the active region, the diffracted field persists out to several hundred kilometers, dropping a further 40 dB at this range – see Fig. 19. [This behavior suggests that when a storm passes over an OBS site in shallow waters characterized by a soft bottom, the seismic response will display dramatic changes as the inhomogeneous component comes in and out of play. When it is inside the active region the OBS will respond to the action of the incident inhomogeneous field as particles close to the interface move in an elliptical orbit. When outside the active region, however, the driving force for the vertical movement no longer exists (we are not dealing here with free internal gravitational waves), and the displacement associated with the inhomogeneous component will quickly die out in a distance of the order of a wavelength.]

Figure 20 presents the same information for the model involving a solid half-space—MD1(1). Since for this model the pole of the bottom-response function is located in the homogeneous wave region, the inhomogeneous component of the pressure field generates only a weak response at the interface and the difference between level (2) (–94.5 dB) representing the response to the total pressure field, and level (3) (–94.6 dB) corresponding to the homogeneous component alone, (equivalent to the bottom "magnification" for the vertical geophone defined in Ref. 10) is only 0.1 dB in this case—see also the plot for MD1(1) in Fig. 8. The calculated spectral level for a region of finite size is again given by curve (1). Inside the active region the seismic response appears to be some 10 dB lower than that for a region of infinite size, level (2). This is however simply a consequence of the size assumed for the finite active region. Because the dominant contribution in this model comes from the homogeneous component, the size of the active region used in the present calculation is not sufficiently large, compared with the wavelengths involved in the homogeneous field, to produce a closer agreement. This contrasts with the case of the liquid bottom discussed above.

The symbols "+ +" in Fig. 20 indicate the range dependence of the spectral level, predicted on the basis of the far-field approximation:

$$F_{mv}^{(2)}=A(f,r)\,|E_v(ur)|^2e^{-2\eta r}/r$$

in which only a single Rayleigh pole is considered. Here, η is the attenuation coefficient of the Rayleigh wave, $\eta=(\omega/2c_r)Q_r^{-1}$, Q_r^{-1} is the linear combination of Q_{a2}^{-1} and Q_{b2}^{-1}, i.e., $Q_r^{-1}=BQ_{a2}^{-1}+(1-B)Q_{b2}^{-1}$, c_r is the Rayleigh wave phase velocity, and B a constant determined by the model parameters.[24] The term $A(f,r)$ involving the wave spectrum and bottom impedance can be readily established by using the residual theorem.[13] As expected, curve (1) tends to the far-field approximation at large distances.

Figures 21 and 22 present the results for the multilayered models (MDK1 and MDK2), assumed to approximate the limits of the real environment in the New Zealand experiment. In both cases the calculated response to the total pressure field inside the restricted active region [curve (1)] is close to that estimated in Sec. II for an active region

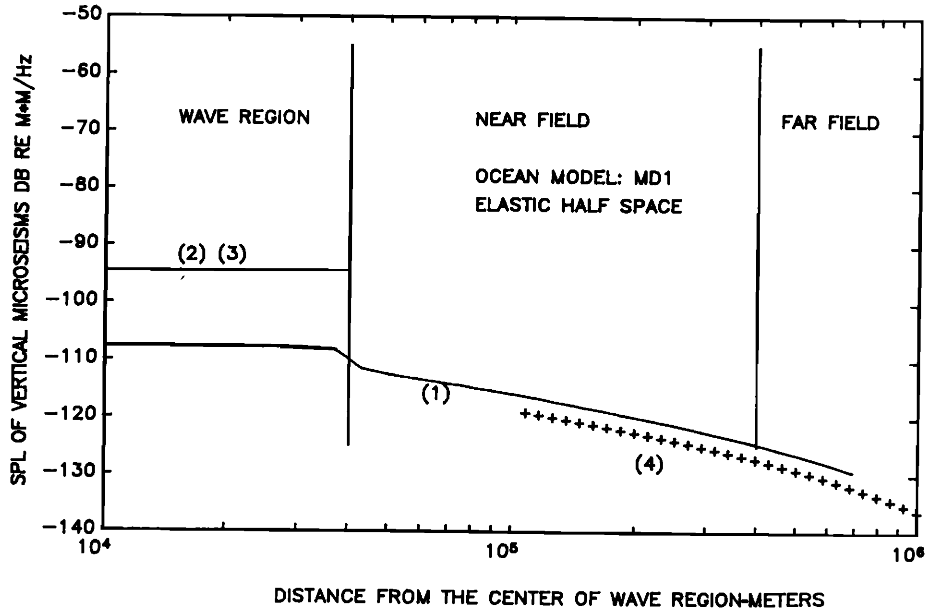

FIG. 20. Decay of the vertical seismic spectral level with distance from the center of the active region, above an elastic half space.

of infinite size [curve (2)]. The level again drops quickly as the observation point is moved just outside the region, to decay more slowly at larger distances. The difference between levels (2) and (3) again demonstrates the relative importance of the homogeneous component in the two models. As mentioned earlier MDK1 represents one model extreme, in which the shear-wave speed in the bottom is taken to be very low, while MDK2 represents the other extreme with high shear-wave velocities defined by the compressional wave-speed profile (see Table I) established from actual geophysical survey data. The difference can obviously be significant, and, as Fig. 21 shows, is nearly 30 dB for this model. In the transition zone outside the active region, the spectral levels in the two models differ by about 10 dB. This is also a result of the difference in the bottom rigidities.

VI. TRANSFER FUNCTIONS AND SOURCE LEVELS ASSOCIATED WITH WAVE-WAVE INTERACTIONS

We now return to the question raised by Schmidt and Kuperman[10] relating to the influence of the "magnification" effect on the New Zealand spectra and the implication this has for the actual source level associated with the wave interaction process.[3,4]

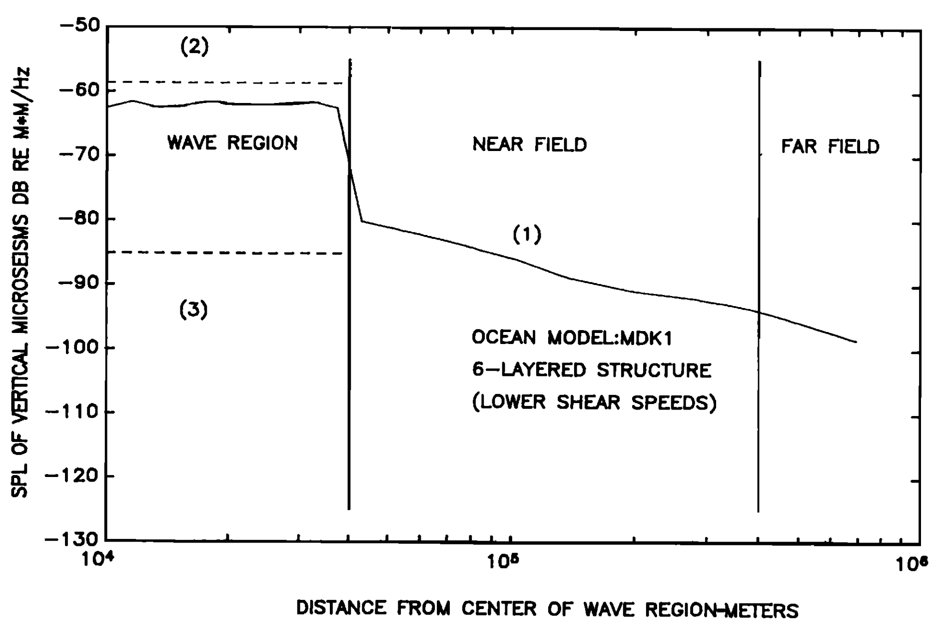

FIG. 21. Decay of the vertical seismic spectral level with distance from the center of the active region for a multilayered bottom characterized by low shear-wave speeds.

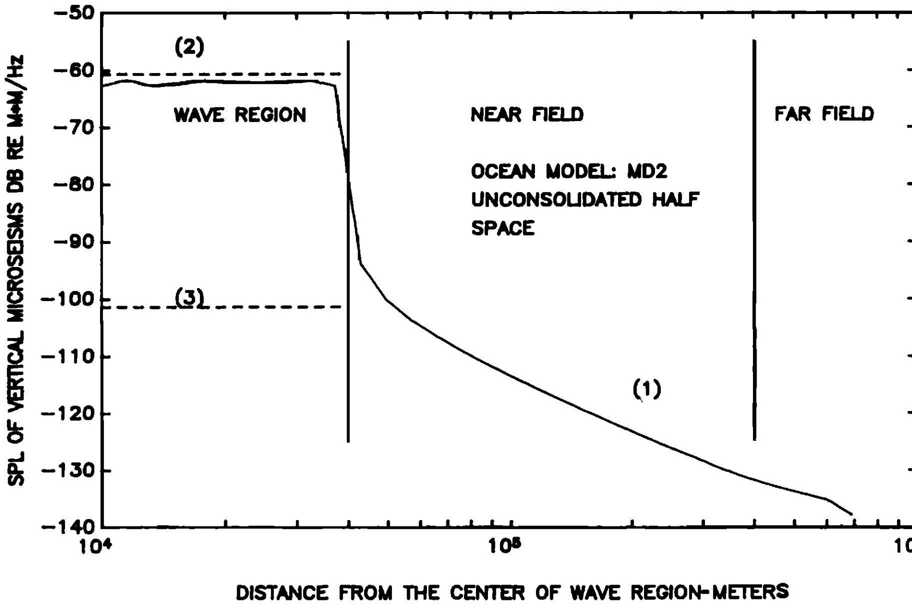

FIG. 22. Decay of the vertical seismic spectral level with distance from the center of the active region for a multilayered bottom characterized by high shear-wave speeds.

The theoretical analysis presented in Sec. I shows that the noise source levels defined in Ref. 10 are essentially those associated with the homogeneous component of the pressure field arising from the wave–wave interaction process. In this case the "magnification" defined in Ref. 10 is simply the ratio of the response to the total pressure field (both the homo- and inhomogeneous components) to that of the homogeneous component alone. This analysis has also confirmed the point however, that the inhomogeneous component of the source can become dominant in many practical situations involving shallow-water environments. Accordingly, in deriving noise source levels from seismic measurements it is necessary to make the appropriate allowance for the "magnification" arising from the contribution from the inhomogeneous component. It has been shown, moreover, that in doing so considerable care must be taken in ascribing values to the relevant model parameters, and in ensuring that adequate numerical accuracy is used. [As we noted earlier the levels of curve (3) for models MDK1 and MDK2 differ by as much as 15 dB, only because of the difference in the shear-wave velocities allocated.]

In Sec. II we discussed the spectral transfer function relating the seismic spectrum measured outside the active region to a specified source pressure field within it. This transfer function is here defined as the ratio of $F_{mv}(\omega,r)$, Eq. (11), to $F_{pr}(\omega)$, Eq. (18), i.e., in terms of the homogeneous component of the pressure field:

$$T_{mp}(\omega,r)=\frac{(\rho_1\alpha_1\omega_1)^2}{C(\omega,r)}, \tag{23}$$

where

$$C(\omega,r)=\frac{\omega^4}{4\pi^3\alpha_1^4 I(\omega)}\int_0^{u_{\max}} |E_p|^2 \times\left[\int_0^{2\pi} |\Gamma_v(u,\theta_k)|^2 I^{(2)} \times(u,\theta_k,\omega)\, d\theta_k\right] u\, du. \tag{24}$$

The factor $C(\omega, r)$ is a function of the geoacoustical structure and the distance from the active region. The transfer functions for the models MDK1, MDK2, and MD2 (based on this definition) are plotted in Fig. 23. Also shown is the simplified transfer function, KE, used by Kibblewhite and Ewans to establish the wind-dependent noise-pressure spectra in Ref. 3. Since the size of the active region used in the calculation was sufficiently large, the curves presented for these three models can be taken to represent a reasonable approximation of the real situation. The figure can be explained simply in the following way. Let us assume a given value of the seismic spectrum level is measured outside the active region. Then if the bottom is a liquid (MD2) the source level of the pressure field must be relatively high to generate the observed seismic response and the high value of the transfer function for this model at a given range reflects this fact. In the case of the multilayered structures MDK1 and MDK2 on the other hand, many interface and body-wave modes carry energy to the seismic sensor so that a lower source level is required to generate the observed seismic response. The values of the transfer function are accordingly lower. Further since MDK2 is acoustically "harder" than MDK1 the higher values of the transfer function for this model are to be expected.

We next turn to the question of source level and first

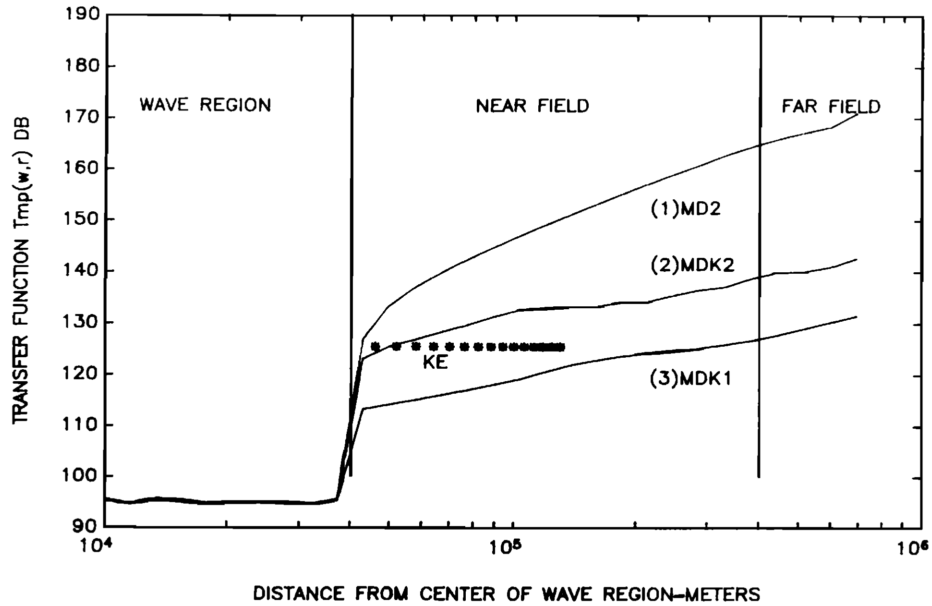

FIG. 23. Variation of the spectral transfer function with distance from the center of the active wave region for various models.

recall that the transfer function KE($=126.3$ dB) was that used in Ref. 3 to establish the wind-dependent pressure spectra from the seismic response measured on shore, just outside the active region. We next note that in this experiment the seismic level recorded (around 0.22 Hz) for a wind speed of 30 m s^{-1} was -85.5 dB *re*: m^2/Hz [-34.5 dB *re*: $(\mu m)^2$/Hz]. This level is 25 dB lower than the theoretical response predicted for this wind speed inside an active region with a water depth of 100 m (~ -60 dB *re*: m^2/Hz). This difference in level is in line with the behavior presented in the plots in Figs. 21 and 22 and confirms that the measured response outside the active region is not markedly influenced by the inhomogeneous component. However using the measured seismic level with the value 126.3 dB for the transfer function leads to a source pressure field inside the active region of about 40 dB *re*: Pa^2/Hz, which is some 10 dB higher than the deep-water value (corresponding to the homogeneous component of the pressure field) expected for this wind speed—see Fig. 6(a) of Ref. 12. This is not surprising given the simplicity of the model and the fact that no propagation effects are included. The situation improves with the multilayered models MDK1 and MDK2. At a nominal distance of 10 km outside the active region, the transfer function ranges from around 115 to 125 dB (close to the KE value). For the observed seismic level (-85.5 dB *re*: m^2/Hz) the predicted source pressure field at 0.22 Hz then ranges from about 30 to 40 dB *re*: Pa^2/Hz.

The geophysical data for the region do not allow the properties of the seabed to be defined with certainty. However it is clear that an inversion based on the more likely model MDK1 (low shear-wave speeds) leads to a value very close to the theoretical pressure field predicted at the frequency (0.22 Hz) and wind speed (30 m s^{-1}) involved, namely 32 dB *re*: Pa^2/Hz—see Fig. 6(a) of Ref. 12. Variation in the water depth over the active region can however also effect the interpretation. The active region lies on edge of the continental shelf and 100 m is a nominal depth only for the region.

Even given these uncertainties it can be concluded that:

(i) The effects of "magnification" discussed in Ref. 10 are incorporated in the calculation of $T_{mp}(\omega,r)$. Using the appropriate value of the transfer function thus reliably establishes a source level from seismic spectra measured at any observation site relative to the active region.

(ii) Because the simple transfer function originally used in Ref. 3 does not differ significantly from that established by the detailed analysis outlined above, the New Zealand wind-dependent pressure spectra are, albeit fortuitously, not significantly distorted by the effects outlined in Ref. 10.

(iii) The fact that the wind-dependent source spectra established in Ref. 3 agree closely in level (to within 10 dB) and in form with those predicted theoretically for the classical wave interaction process, and almost exactly using model MDK1, is further significant evidence that this process is indeed the source of the peak in the ULF noise spectrum. This conclusion is reinforced by predictions based on other theoretical developments recently presented by Cato [25,26] and Lindstrom.[27]

We acknowledged in an earlier paper[8] that any conversion between pressure and seismic spectra should properly involve transfer functions based on the complete multi-layered structure and must reflect any effects the finite size of the active region might have in the near field. The nature of these effects has been established above, but before this evaluation was available it was only possible to make the rough approximation using simplified models, as reported in Refs. 3, 8, and 9. The approximation used in Ref. 3 is the simplest possible, assuming as it does an unconsolidated half-space. We can now see why the inversion based on this model agrees with the theoretical predictions for the more complex model to within a few decibels. The subject is however indebted to Schmidt and Kuperman for highlighting the importance of these issues.

Another factor, which can influence the theoretically derived noise source levels, is the wave-spreading function, included in the factor $I^{(2)}(u,\theta_k,\omega)$. We made a limited analysis of the influence of this parameter in Ref. 9 but acknowledge it requires further attention. We note however that the spreading function is not dependent on the environment and it is the environmental influences which have been of concern in this paper. Accordingly we have used the traditional representation of the spreading function in this analysis. The neglect of the dependence of $I^{(2)}(u,\theta_k,\omega)$ on the wave number, u, when u is close to its upper limit, $\omega\alpha_1/g$, will introduce some errors at very low frequencies, but we believe the general thrust of the analysis presented in the previous sections cannot be substantially altered by the spreading function. In a subsequent paper we will discuss these points in more detail, including a discussion of the properties of the spatial correlation of the generated ULF noise field.

VII. SUMMARY

This paper was prompted by the apparent implications of an analysis recently reported by Schmidt and Kuperman. In this they draw attention to the enhanced noise spectral levels which can arise at low frequencies in shallow water environments due to bottom interaction effects. On the basis of these results they questioned whether the characteristics of wind-dependent noise spectra reported from a New Zealand experiment were not due simply to this bottom magnification rather than nonlinear wave–wave interactions as claimed. This paper addresses the issues raised.

The theoretical basis of the microseism response induced by the nonlinear interaction of surface gravitational waves has been carefully examined. A general expression for the seismic spectrum as a function of the size of the active region and the range from the region is established for a multi-layered viscoelastic environment. When the size of the active wave region tends to infinity this general formula is shown to simplify to the classical form derived for an active region of infinite size. The relative importance of the homogeneous and inhomogeneous components of the source and the nature of the medium response are examined in detail for typical geoacoustical models.

The physical upper limit of the horizontal wave number, $u_{\max}$, is introduced for the first time into the theoretical expression for the wave-induced microseismic spectra. At very low frequencies and near the surface this limit has the value $\omega\alpha_1/g$, while at high frequencies it assumes the value of $4.5\alpha_1/\omega h_1$. In the general case $u_{\max} = \min[\omega\alpha_1/g, 4.5\alpha_1/\omega h_1]$. The first of the two limits is controlled by the wave number of the interacting surface waves and the second by the factor describing the exponential decay of the inhomogeneous field with increasing water depth, h_1. The existence of such an upper limit to the relative horizontal wave number, u, establishes a high peak in the spectral transfer function relating the source pressure field to the microseismic field, at around 0.05 Hz.

The relative importance of the homogeneous and inhomogeneous components to the seismic response is shown to be critically dependent on the geoacoustic model, especially on the values of the geoacoustical parameters of the top sedimentary layer. When the top layer is an unconsolidated sediment (or one of low rigidity) the total spectral level can be up to 40 dB higher than the spectral level produced by the homogeneous component alone. The shear-wave speeds in the sublayers and the thickness of the water layer are also shown to have a significant influence on the relative importance of these two components.

The Green's functions for four representative models have been calculated numerically to reasonably high accuracy. Based on these Green's functions the seismic response in the near-field region to nonlinear interactions in the ocean-wave field is calculated for the first time. It is found that high spectral levels are associated with the inhomogeneous component in a shallow water region with a soft bottom, but that these quickly decrease as the observation point moves outside the finite active region (or as a storm region moves away from a sensor sitting on the bottom). In the case of an unconsolidated half-space it is shown that the total level can drop by as much as 40 dB in crossing the boundary of the active region, and that thereafter it decays approximately as r^{-2} (spherical spreading) to large distances. In this case the seismic field outside the wave region can thus be recognized as the diffraction field of the homogeneous component, which is insonifying a bottom "plate" of finite size. In the case of a solid bottom the near-field spectral level is shown to decay more slowly and to tend to that predicted by the far-field approximation based on the free Rayleigh wave mode. In the multilayered case the spectral level in the transition region decays as r^{-1} and shows the effects of the interface wave propagation. The extreme cases of high and low shear speeds differ in spectral level by about 10 dB in this region.

The suggestion made in Ref. 10 that the wave interaction source spectrum levels derived in Ref. 3 may be 40–50 dB too high is examined in the light of these results, and the general validity of the New Zealand spectra is confirmed. It is shown that the value of the transfer function used in Ref. 3 is (albeit fortuitously) a reasonable approximation of the real transfer function, so that the general conclusions reached in Ref. 3 relating to the wave interaction noise generation process can be confirmed. However, while the New Zealand spectra are no doubt correct in their general form, changes in detail can be expected with changes in frequency, wind speed, ocean-wave spectral form and the wave spreading functions. Further, convincing as the analysis of the New Zealand situation appears to be, it must not be overlooked that the geophysical structure of Cook Strait is very complex and not well known. While the deep structure does not appear to influence the seismic response greatly, it will be pleasing to see the close agreement between theory and experiment confirmed by similar results from deep-water sites.

ACKNOWLEDGMENTS

The authors wish to express their thanks to the Computer Center of the University of Auckland for their sympathetic support in the long and tedious numerical calculations, and to Dr. M. D. Johns and Dr. S. M. Tan of the Department of Physics for their help and cooperation at all times.

This work was supported by the U.S. Office of Naval Research under Contract No. 00014-89-J-3130/P00002 and N00014-92-J-1037.

APPENDIX A: THE ERROR TERM

In the calculation of the microseismic spectra in terms of Eq. (11), the error term caused by truncation of the wave number in the calculation of the Green's function can be written as:

$$\mathscr{E}(\omega,r)=A(\omega)\int_0^\infty H(u)\left| E_p(u)\int S(\xi_0) \times\left[\int_0^\infty \bar{H}(\tilde{u})ff_v(\tilde{u})J_0(\xi\tilde{u})\,\tilde{u}d\tilde{u}\right] \times e^{iu\xi_0}\,d\xi_0\right|^2 u\,du, \tag{A1}$$

where $H(u)$ and $H(\tilde{u})\equiv 1$ when $0\leqslant u$, $\tilde{u}\leqslant u_{\max}$, $\bar{H}(\tilde{u})=1-H(\tilde{u})$, $\xi_0=\mathbf{r}_0\,\omega/\alpha_1$, and $\xi=\mathbf{r}\,\omega/\alpha_1$. The term $I(u,\theta_k,\omega)$ has been assumed to be constant. We first consider the case when the observation point is at the center of the active region. By introducing expressions $\delta(u-u')=\sqrt{u\,u'}\int_0^\infty J_0(pu')J_0(pu)p\,dp$, and $H(u)=H^2(u)$ into (A1) and assuming the active wave region to be of infinite size with a Gaussian weight $\exp[-(\xi_0/\xi_e)^2]$ we can write

$$\mathscr{E}(\omega)=4\pi^2A(\omega)\int_0^\infty |I(p)|^2p\,dp,$$

where

$$I(p)=\int_0^\infty\int_0^\infty H(u)\bar{H}(\tilde{u})\,E_p(u)\,ff_v(\tilde{u})\,g(u,\tilde{u}) \times J_0(pu)\,u\tilde{u}\,du\,d\tilde{u} \tag{A2}$$

and

$$g(u,\tilde{u})\equiv\int_0^\infty J_0(\xi_0\tilde{u})J_0(\xi_0u)e^{-(\xi_0/\xi_e)^2}\xi_0\,d\xi_0 =\tfrac{1}{2}\xi_e^2I_0(\tfrac{1}{2}\xi_e^2u\tilde{u})e^{-\xi_e^2(u^2+\tilde{u}^2)/4}.$$

The integration of (A2) in the shadowed region (see Fig. A1) corresponds to the error term. It is seen that when the size of the region (the equivalent radius ξ_e) tends to infinity, $g(u,\tilde{u})$ becomes a δ function of $(u-\tilde{u})$, and the error term is zero. In the case of a region of finite size and an observation point located in the center of the source region, it can be shown that the dominant term in the integration over $\tilde{u}$ in Eq. (A2) [assuming $ff_v(\tilde{u})\sim\tilde{u}$], viz.,

$$\bar{I}_u=\frac{c\xi_e^2}{2}\int_{U_{\max}}^\infty I_0\left(\frac{1}{2}\xi_e^2u\tilde{u}\right)e^{-\xi_e^2(\tilde{u}^2+u^2)/4}\tilde{u}^2\,d\tilde{u}$$

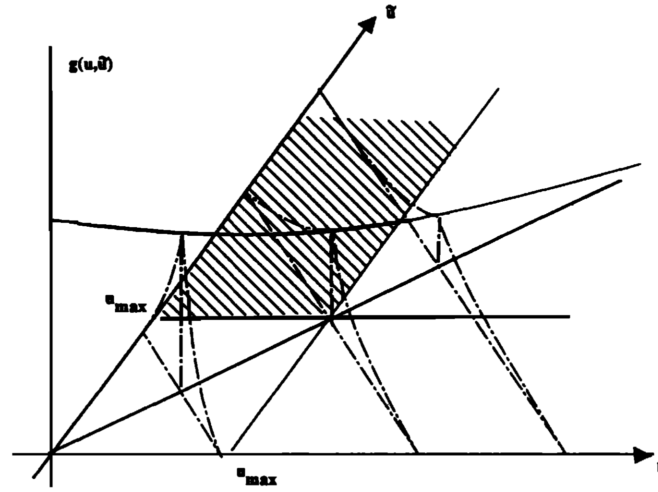

FIG. A1. Sketched plot of the function $g(u,\tilde{u})$ on the plane $(u\tilde{u})$.

is [through using the relation $I_0(x)\sim\exp(x)/(2\pi x)^{1/2}<\exp(x)$ large x, and carrying out the integration]

$$c(\sqrt{\pi}/2)\,\xi_eu^2\{1-\Phi[\tfrac{1}{2}\xi_e(u_{\max}-u)]\}$$

for

$$\xi_e\,u_m\gg 1$$

while the integration along the whole axis ($\tilde{u}=0$ *to* ∞) can be estimated as [if we take $ff_v(u)=\text{const}$]

$$I_u=\frac{c\xi_e^2}{2}\int_0^\infty I_0\left(\frac{1}{2}\xi_e^2u\tilde{u}\right)e^{-\xi_e^2(\tilde{u}^2-u^2)/4}\tilde{u}^2\,du =\frac{c\sqrt{\pi}}{\xi_e}\left[I_0\left(\frac{1}{8}u^2\xi_e^2\right)+I_1\left(\frac{1}{8}u^2\xi_e^2\right)\right]e^{(3/8)u^2\xi_e^2} \geqslant\frac{c\sqrt{\pi}}{\xi_e}e^{(3/8)u^2\xi_e^2}.$$

The ratio $\bar{I}_u/I_u$ will thus decay exponentially with increasing u and the size of the active region. When the observation point is separated from the center by a distance r by using the addition theorem for cylindrical functions, we can write

$$g_r(u,\tilde{u})\equiv J_0(\xi_r\tilde{u})g(u,\tilde{u})+2\sum_{m=1}^\infty i^mJ_m(\xi_r\tilde{u})g_m(u,\tilde{u}),$$

where

$$g_m(u,\tilde{u})=\tfrac{1}{2}\xi_e^2I_m(\tfrac{1}{2}\xi_e^2\tilde{u}u)e^{\xi_e^2(u^2+\tilde{u}^2)/4}.$$

Since for $m\geqslant 1$, $I_m(x)$ is equal to zero when $x=0$, and has the same asymptotic expression for $x\gg 1$, we can write

$$g_r(u,\tilde{u})\cong g(u,\tilde{u})\left|J_0(\xi\tilde{u})+2\sum_{m=1}^\infty i^mJ_m(\xi\tilde{u})\right| =g(u,\tilde{u})e^{i\xi\tilde{u}/\sqrt{2}}.$$

This means that in Fig. A1 the exponential function becomes oscillatory with short periods in the shadowed region. It is thus anticipated that the ratio $\bar{I}_n/I_u$, will keep decreasing as the distance r increases.

APPENDIX B: THE EXPRESSION $I^{(2)}(U,\theta_k,\omega)$

As derived in Ref. 12, we have

$$I^{(2)}(u,\theta_k,\omega)=\int_0^{2\pi}\frac{[1-\cos(\theta_1-\theta_2)]^2\chi^2}{(1+\chi)^2(1-\frac{1}{4}\hat{m}^2)[\chi^2-(\frac{1}{2}\hat{m}\hat{t}+1)\chi+(1-\frac{1}{2}\hat{m}\hat{t})]}$$

$$\times\frac{F_a[\omega/(1+\chi)]F_a[\chi\omega/(1+\chi)]}{F_a^2(\omega/2)}H(\theta_2-\theta_\omega)H(\theta_2-\theta_\omega)d\theta_1,$$

where

$$\hat{m}=2kg/\omega^2,$$

$$\hat{t}=\cos(\theta_1-\theta_k)$$

$$\theta_2=\theta_1-(\pi-\psi)\operatorname{sgn}[\sin(\theta_1-\theta_k)]$$

$$\psi=\cos^{-1}\left(\frac{1-\frac{1}{2}\hat{m}\hat{t}(1+\chi)^2}{\chi^2}\right).$$

Here, θ_ω is the wind direction, $H(\theta)$ is the normalized wave directional energy distribution, and χ is the solution of a cubic equation $(\chi^2+1)(\chi-1)-\frac{1}{4}\hat{m}^2(1+\chi)^3+\hat{m}\hat{t}\times(1+\chi)=0$. In the above $\operatorname{sgn}(x)=x/|x|$.

[1] M.S. Longuet-Higgins, "A theory of the origin of microseisms," Philos. Trans. R. Soc. London Ser. A **243**, 1–35 (1950).

[2] K. Hasselmann, "A statistical analysis of the generation of microseisms," Rev. Geophys. **1**, 177–210 (1963).

[3] A.C. Kibblewhite and K.C. Ewans, "Wave–wave interactions, microseisms and infrasonic ambient noise in the ocean," J. Acoust. Soc. Am. **78**, 981–994 (1985).

[4] A.C. Kibblewhite and K.C. Ewans, "A study of ocean and seismic noise at infrasonic frequencies," *Ocean-Seismo Acoustics Series IV*, edited by T. Akal and J.M. Berkson (Plenum, New York, 1986), Vol. 16, pp. 731–741.

[5] S.C. Webb and C.S. Cox, "Observations and modelling of seafloor microseisms," J. Geophys. Res. **91**, 7343–7358 (1986).

[6] R.G. Adair, "Microseisms in the deep ocean: observations and theory," Doctoral dissertation, University of California at San Diego, La Jolla, CA (1985).

[7] R.G. Adair, J.A. Orcutt, and T.H. Jordan, "Low frequency noise observations in the deep ocean," J. Acoust. Soc. Am. **80**, 633–645 (1986).

[8] A.C. Kibblewhite and C.Y. Wu, "The generation of infrasonic ambient noise in the ocean by nonlinear interactions of ocean surface waves," J. Acoust. Soc. Am. **85**, 1935–1945 (1989).

[9] A.C. Kibblewhite and C.Y. Wu, "A re-examination of the role of wave–wave interactions in ocean noise and microseisms," J. Acoust. Soc. Am. **85**, 1946–1957 (1989).

[10] H. Schmidt and W.A. Kuperman, "Estimation of surface noise source level from low-frequency seismoacoustic ambient noise measurements," J. Acoust. Soc. Am. **84**, 2153–2162 (1988).

[11] M.A.H. Hedlin and J.A. Orcutt, "A comparative study of island, sea floor, and sub-sea floor ambient noise levels," Bull. Seis. Soc. Am. **79**(1), 172–179 (February 1989).

[12] A.C. Kibblewhite and C.Y. Wu, "The theoretical description of wave–wave interactions as a noise source in the ocean," J. Acoust. Soc. Am. **89**, 2241–2252 (1991).

[13] W.M. Ewing, W. Jardetsky, and F. Press, *Elastic Waves in Layered Media* (McGraw-Hill, New York, 1957).

[14] A.C. Kibblewhite, "Attenuation of sound in marine sediments: A review with emphasis on low-frequency data," J. Acoust. Soc. Am. **86**, 716–738 (1989).

[15] M.B. Priestley, *Time Series and Spectral Analysis* (Academic, New York, 1981), Vol. 1, Univaric series.

[16] D.S. Jones, *Generalized Functions* (McGraw-Hill, New York, 1966).

[17] W.A. Kuperman and F. Ingenito, "Spatial correlation of surface generated noise in a stratified ocean," J. Acoust. Soc. Am. **67**, 1988–1996 (1980).

[18] H. Schmidt, "Numerical modeling in ocean seismoacoustics," Proc. Oceans'91, 1–3 October 1991, Honolulu, Hawaii **1**, 84–92 (1991).

[19] H. Schmidt and F.B. Jensen, "A full wave solution for propagation in multilayered viscoelastic media with application to Gaussian beam reflection at fluid–solid interfaces," J. Acoust. Soc. Am. **79**, 813–825 (1985).

[20] H. Schmidt, "SAFARI: Seismoacoustic fast field algorithm for range dependent environments," User's guide SR 113, SACLANT ASW Research Center, La Spezia, Italy (1987).

[21] C.Y. Wu, "Wave–wave interactions and the infrasonic pressure field in the ocean," Doctoral dissertation, University of Auckland, New Zealand (1988).

[22] K.C. Ewans and A.C. Kibblewhite, "An examination of fetch-limited wave growth off the west coast of New Zealand by a comparison with the JONSWAP results," J. Phys. Oceanogr. **20**(9), 1278–1296 (1990).

[23] L.M. Brekhovskikh, *Waves in Layered Media* (Academic, New York, 1980), 2nd ed.

[24] J.R. MacDonald, "Rayleigh-wave dissipation function in low-loss media," Geophys. J. R. Astron. Soc. **2**, 132–135 (1959).

[25] D.H. Cato, "Sound generation in the vicinity of the sea surface: Source mechanisms and the coupling to the received sound field," J. Acoust. Soc. Am. **89**, 1076–1095 (1991).

[26] D.H. Cato, "Theoretical and measured underwater noise from surface orbital motion," J. Acoust. Soc. Am. **89**, 1096–1112 (1991).

[27] T.E. Lindstrom, "Predictions and observations of sea floor infrasonic noise generated by sea orbital motion" (private communication, September 1991).